LITHOS 406–407 (2021) 106494

Contents lists available at ScienceDirect

LITHOS

journal homepage: www.elsevier.com/locate/lithos

Regular Article

Magmatic rifting in the Main Ethiopian Rift began in thick continental lithosphere; the case of the Galema Range

B. Chiasera [a,*], T.O. Rooney [a], I.D. Bastow [b], G. Yirgu [c], E.B. Grosfils [d], D. Ayalew [c], P. Mohr [e], J. Zimbelman [f], M. Ramsey [g]

[a] Dept. of Earth and Environmental Sciences, Michigan State University, East Lansing, MI 48824. United States
[b] Department of Earth Science and Engineering, Imperial College London, London SW7 2AZ, UK
[c] Dept. of Earth Sciences, Addis Ababa University, Addis Ababa, Ethiopia
[d] Dept. Geology, Pomona College, Claremont, CA, United States
[e] Tonagharraun, Corrandulla, Ireland
[f] CEPS MRC 315, Smithsonian Institution, Washington D.C., DC, United States
[g] Dept. Geology & Planetary Science, University of Pittsburgh, Pittsburgh, PA, United States

ARTICLE INFO

Keywords:
Continental rifting
Main Ethiopian Rift
East African Rift system
Mantle potential temperature
Lithosphere-asthenosphere boundary

ABSTRACT

The northern Main Ethiopian Rift (MER) in East Africa is considered a region of incipient oceanic spreading, with Miocene border faulting now largely abandoned at the expense of magmatic extension in the Wonji Fault Belt (WFB). However, whether magmatic extension began when the Ethiopian lithosphere was still-thick, or heavily stretched, is unknown. The Galema range, a linear Pliocene dike swarm parallel to the eastern margin of the present-day central MER, is an ideal study locale to constrain melting depths, and by inference the thickness of the lithosphere, during early magmatic rifting. To address this issue, we present whole-rock, trace element data on 77 samples of Galema range magmas. We interpret contrasting results between two modeling approaches as evidence for magma ponding subsequent to melt generation. Trace element models of melt generation reveal melting conditions of T_P = 1418–1450 °C at 2.9–3.2 GPa, some ~68–100 °C above ambient. In contrast, Si/Mg activity thermobarometry, which probes the point at which these magmas last re-equilibrated with the mantle, yielded broadly similar temperatures (1435–1474 °C) but at lower pressures (2.1–2.6 ± 0.2 GPa: 78–89 km depth); these results are broadly parallel to contemporaneous magmatism on the western rift margin in the Akaki Magmatic Zone. We interpret these results as evidence for magma stalling at a thermo-mechanical boundary to ascent: the lithosphere-asthenosphere boundary. The Ethiopian continental lithosphere has therefore remained relatively thick late into the rifting process, with important potential implications for late-stage decompression melting prior to the onset of seafloor spreading.

1. Overview

There is a growing awareness emerging from studies of rifts and margins worldwide that continental rift magmatism should not be considered simply an extrusive igneous response to decompression of the upper mantle attendant to plate thinning; magma intrusion can accommodate extension prior to the formation of a new ocean basin (e.g., Ebinger and Casey, 2001; Mackenzie et al., 2005; Reeve et al., 2021; Thybo and Nielsen, 2009; White et al., 2008). The existing paradigm envisages that the accommodation of extension by magma intrusion reflects late-stage rifting processes occurring in thin lithosphere prior to ocean basin formation. However, constraints as to where and when during the rifting process the transition from mechanical to magmatic extension occurs, and the thickness of the plate during this transition, are only partially understood.

The Main Ethiopian Rift captures multiple stages of rift sector development, from embryonic continental rifting in the south to incipient oceanic spreading in the north (e.g., Ebinger et al., 2017; Hayward and Ebinger, 1996), above an anomalously slow wavespeed (Bastow et al., 2008; Benoit et al., 2006a; Benoit et al., 2006b; Boyce et al., 2021; Ritsema et al., 1999), hot (e.g., Rooney et al., 2012c) upper-mantle. While southern and central Afar regions to the north of 10°N have been shaped by Cenozoic rifting processes associated with both the Red Sea Rift and near-orthogonal Nubia-Somalia separation, Ethiopia to the

* Corresponding author.
E-mail address: chiasera@msu.edu (B. Chiasera).

https://doi.org/10.1016/j.lithos.2021.106494
Received 17 May 2021; Received in revised form 13 September 2021; Accepted 30 September 2021
Available online 14 October 2021

south of 10°N has been affected only by the latter (e.g., Wolfenden et al., 2004). The Main Ethiopian Rift is thus an ideal study locale for examining magmatic rifting processes.

In the northern Main Ethiopian Rift, the 60-km-long, large-offset Miocene border faults that define rift valley topography no longer accommodate the majority of extension; ~80% of extensional strain is now focused within the Wonji Fault Belt, a relatively narrow (20 km-wide) belt of much shorter length-scale (1 km) faulting and associated magmatism (e.g., Ebinger and Casey, 2001; Mohr, 1967). A suite of geoscientific studies over the past two decades has revealed that the Wonji Fault Belt is underlain by seismically fast (Keranen et al., 2004; Mackenzie et al., 2005), dense (Cornwell et al., 2006) material,

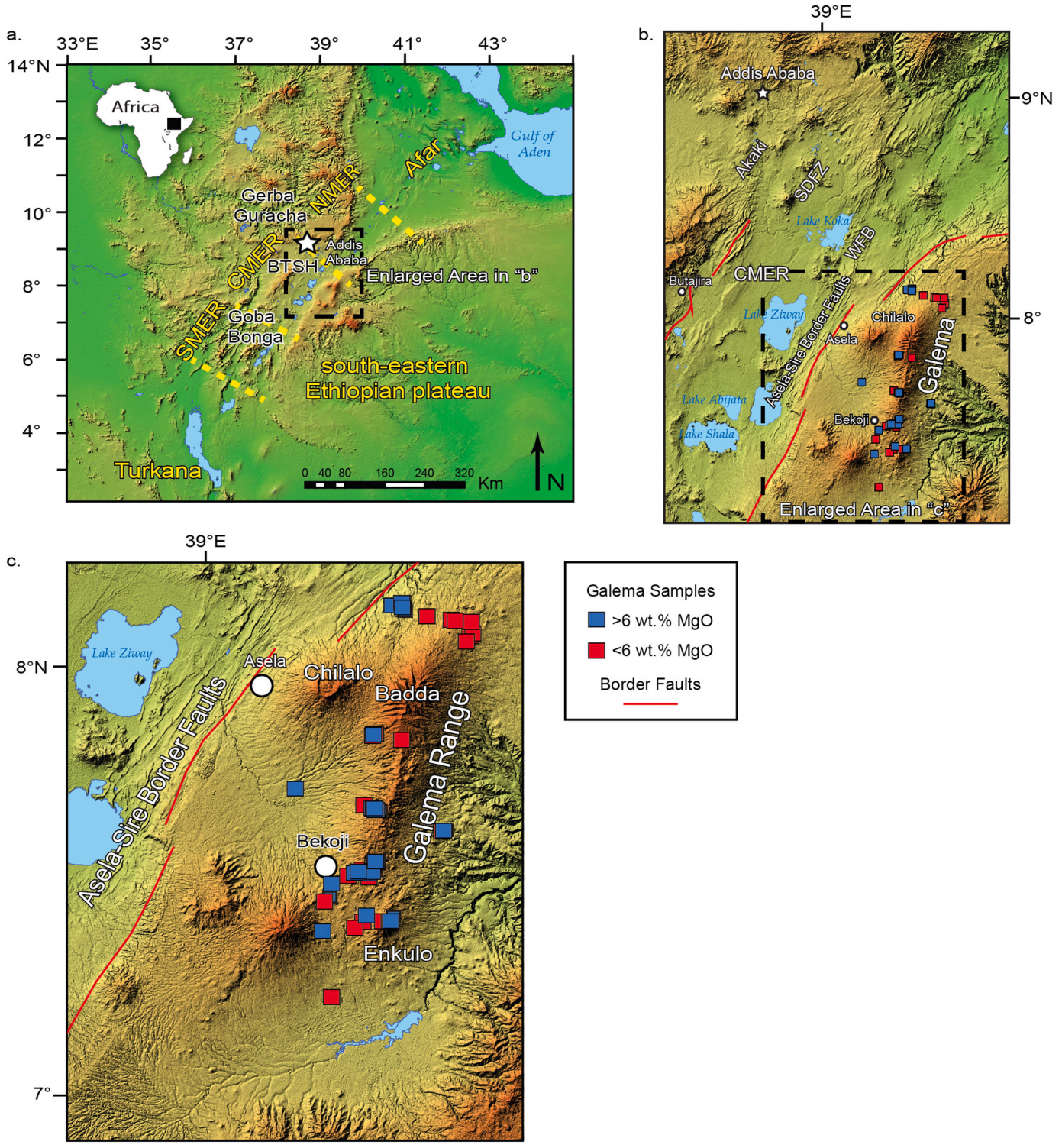

Fig. 1. a. Tectonic setting of the Main Ethiopian Rift (MER) within the East African Rift System (EARS). Northern Main Ethiopian Rift (NMER), Central Main Ethiopian Rift (CMER) and Southern Main Ethiopian Rift (SMER). Dashed line delineates (b). b. The central Main Ethiopian Rift. WFB: Wonji Fault Belt; SDFZ: Silti-Debre Zeyit Fault Zone; AMZ: Akaki Magmatic Zone; YTVL: Yerer-Tullu Wellel Volcanotectonic Lineament. Dashed line delineates (c). c. Enlarged portion of the central Main Ethiopian Rift showing the location of the Galema range and samples used in this study.

interpreted as cooled gabbroic intrusions in the mid-to-upper crust that have accommodated extension without marked crustal thinning since Quaternary times. Melt intrusion is also thought to have accounted for appreciable extension of the mantle lithosphere (e.g., Bastow et al., 2010; Kendall et al., 2005), but commonly applied geophysical methods (S-to-P receiver functions) for estimating plate thickness have proven unable to constrain the lithosphere-asthenosphere boundary depth below the Main Ethiopian Rift (e.g., Lavayssière et al., 2018; Rychert et al., 2012). Such methods would, in any case, provide only a present-day snapshot of rift structure, not its development through time. Whether or not magmatic extension began in still-thick continental lithosphere, or after a major shallowing of the lithosphere-asthenosphere boundary, remains unknown. The challenge is therefore to constrain plate thickness during earlier magmatic rifting phases using evidence from the geological record.

Here we examine the Galema range, a zone of focused magmatism that was emplaced parallel to the eastern margin of the central Main Ethiopian Rift (Mohr and Potter, 1976) (Fig. 1). The Galema range represents a region of focused strain that developed prior to the Wonji Fault Belt (Mohr and Potter, 1976). We present whole-rock geochemical data for 77 samples of magmatic products from the Galema range and use these data to investigate the intensive parameters of melt generation and depths of magma ponding within the asthenosphere. Using a combination of thermodynamic modeling techniques, we confirm previous estimates of relatively high pressures (2.9–3.2 GPa, 103–112 km depth) of melt generation (Chiasera et al., 2018) and demonstrate, for the first time, that the melts were generated in the asthenosphere at relatively high temperatures (1418–1450 °C) but stalled during ascent and re-equilibrated below a thick (78–89 km) lithosphere, prior to intrusion. These results reveal that magmatic extension occurred in still-thick lithosphere beneath the margin of the East African rift, prior to the development of the progressively rift-axial zones of short length-scale faulting and magmatism that mark the present-day locus of extensional strain.

2. Background

2.1. Cenozoic magmatic evolution of the African-Arabian Large Igneous Province

Cenozoic magmatic activity in East Africa commenced in the Eocene with a pulse of flood basalt magmatism in the broadly-rifted Turkana Depression (northern Kenya) and throughout southern Ethiopia (Davidson and Rex, 1980; Ebinger et al., 1993; Furman et al., 2006b; George et al., 1998; Stewart and Rogers, 1996). Subsequent magmatic activity during the Oligocene migrated northward with eruption of flood basalts across Ethiopia (Baker et al., 1996; Beccaluva et al., 2009; Hofmann et al., 1997; Kieffer, 2004; Krans et al., 2018; Natali et al., 2016; Pik et al., 1999; Rochette et al., 1998; Rooney et al., 2018). Early Miocene volcanism occurred broadly throughout the region, with shield building and fissure-fed basalts on the eastern and western Ethiopian Plateaus (e.g., Kieffer, 2004; Nelson et al., 2019), and the Samburu and Getra Kele basaltic events in southern Ethiopia and northern Kenya (Ebinger et al., 2000; George and Rogers, 2002; Hackman, 1988; Rooney, 2020a).

Subsequent volcanic activity took the form of large volume basaltic pulses in the Mid-Miocene and Pliocene, separated by chemically more-evolved episodes (Abebe et al., 1998; Abebe et al., 2005; Ayalew et al., 2018; Bellieni et al., 1986; Chernet et al., 1998; Corti et al., 2019; Dunkley et al., 1993; Haileab et al., 2004; Kieffer, 2004; Mohr and Zanettin, 1988; Rooney, 2020a, 2020b; Ukstins et al., 2002; Woldegabriel et al., 1990; Wolfenden et al., 2004; Wolfenden et al., 2005). Modern magmatism within the eastern branch of the East African Rift System manifests as zones of focused magmatic intrusion (Ebinger and Casey, 2001). Within the Main Ethiopian Rift, these zones of focused magmatic intrusion and tectonism are termed the Wonji Fault Belt and Silti-Debre Zeyit Fault Zone, together characterized by a series of en-echelon dikes, lava flows, scoria cones, and associated silicic centers (Kurz et al., 2007; Mohr, 1967; Mohr et al., 1980; Rooney et al., 2005; Woldegabriel et al., 1990) (Fig. 1). Within the relatively thinner crust of the northern MER (Maguire et al., 2006), the Wonji Fault Belt is approximately rift-axial; in the less-evolved central Main Ethiopian Rift, with its thicker crust, the Silti-Debre Zeyit Fault Zone and Wonji Fault Belt, respectively, occur along the western and eastern rift margins.

The temporal evolution described above points to the Pliocene – Quaternary transition as an important period during which magmatism within the rift valleys of the East African Rift System became more focused. For example, Pliocene-Quaternary magmatism occurring in the Afar region, known as the Gulf Series (Rooney, 2020b), represents a shift in magmatism from broadly distributed lava flows of the preceding Afar Stratoid Series toward focusing of extensional strain accommodation (Daoud et al., 2010; Daoud et al., 2011; Kidane et al., 2003; Lahitte et al., 2003; Le Gall et al., 2015; Stab et al., 2015). Such Pliocene-Quaternary magmatism also occurred on the margins of the central Main Ethiopian Rift, and is best represented by the Akaki Magmatic Zone along the western margin (Rooney et al., 2014) as well as the Galema range along the eastern margin (Mohr, 1980; Mohr and Potter, 1976) (Fig. 1).

2.2. The Galema Range

The Galema range, located on the eastern Ethiopian plateau in the central Main Ethiopian Rift (Fig. 1), is an area of focused magmatic intrusion and associated volcanism. Magmatic activity in the Galema Range manifests as en-echelon mafic dikes, aligned scoria cones, and associated silicic centers (Chiasera et al., 2018; Mohr, 1980; Mohr and Potter, 1976). Geochronological, K-Ar estimates place magmatism of the Galema range within the Pliocene-Quaternary boundary, dating from 2.1 to 3.1 Ma (Kennan et al., 1990; Mohr and Potter, 1976). Though it is located on the rift shoulder, the magma plumbing system architecture of the Galema range has been linked to the same extensional stresses that formed other extensional features of the central Main Ethiopian Rift, such as the Wonji Fault Belt and Silti-Debre Zeyit Fault Zone (Fig. 1) (Chiasera et al., 2018). Thermobarometric analyses of clinopyroxene-liquid pairs from the Galema range basalts, combined with thermodynamic MELTS modeling, have revealed that the magma plumbing system of the Galema range is polybaric, with magma stalling within the lithosphere at ~11 and ~25 km, at a maximum temperature of 1307 °C (Chiasera et al., 2018). This is consistent with determinations of magma plumbing system architectures elsewhere in the region, such the Silti-Debre Zeyit Fault Zone, the Akaki Magmatic Zone, and the Wonji Fault Belt; these were formed as a result of magma overpressure interacting with regional extensional stresses (Chiasera et al., 2018; Iddon and Edmonds, 2020; Mazzarini et al., 2013a; Peccerillo et al., 2003; Rooney et al., 2007; Trua et al., 1999).

As the magmatic locations, such as the Gademsa and Boset volcanic complexes, are considered to be part of the larger Wonji Fault Belt within the rift (e.g., Mohr, 1967), magmatic centers such as Chilalo, Bada, and the Galema range may be part of a larger magmatic system on the southeastern Ethiopian plateau (e.g., Mazzarini et al., 2013a; Mazzarini et al., 2013b). These nearby areas of magmatic activity would have been generated within the same conditions as those of the Galema range, such as mantle potential temperature and melt generation depth.

2.3. Geophysical constraints on Ethiopian plate thickness

The highest resolution geophysical images of lithospheric architecture in Ethiopia come from wide-angle seismic profiles (e.g., Mackenzie et al., 2005). Both along- and across-rift reflection-refraction experiments conducted during the 2001–2003 EAGLE experiment reveal a mid-lithosphere reflector 10-25 km beneath the Moho under the Main Ethiopian Rift and surrounding plateau regions (e.g., Maguire et al., 2006). This 'L' mantle reflector was interpreted by Maguire et al. (2006)

as a compositional or structural boundary within lithosphere. Owing to the correlation of the 'L' reflector's depth with the amount of crustal extension along both the cross- and along-rift profiles, Maguire et al. (2006) concluded it was likely a feature that pre-dated Cenozoic rifting and hotspot tectonism. Unfortunately, the wide angle profiles in Ethiopia do not penetrate greater depths, so passive seismic analysis of the seismograms of distant earthquakes are required for deeper imaging.

Receiver function analysis seeks to identify P-to-S or S-to-P converted energy from velocity discontinuities (e.g., the Moho and lithosphere-asthenosphere boundary) beneath a seismograph station (e.g., Langston, 1979). Such techniques work well when the velocity gradient concerned is steep, but cannot necessarily identify boundaries if they are defined by gradational changes in wavespeed (Eaton et al., 2009; Gallacher and Bastow, 2012). In contrast, surface wave analysis of lithosphere-asthenosphere boundary depth does not rely on the presence of sharp wavespeed boundaries; depths are constrained instead by first constraining a velocity-depth profile below a region, then inferring the depth of the lithosphere-asthenosphere boundary using a velocity anomaly proxy (e.g., the 1.7% fast velocity contour: e.g. Darbyshire and Eaton, 2010).

Accordingly, lithosphere-asthenosphere boundary depth has been explored seismically in Ethiopia via continent-scale surface wave analysis (<80 km; e.g., Priestley et al., 2008; Fishwick and Bastow, 2011), and joint inversion of surface waves and P-to-S receiver functions (60–80 km; Dugda et al., 2007). Modeling azimuthal variations in Love and Rayleigh wavespeeds across the Main Ethiopian Rift, Bastow et al. (2010) constrained an oriented melt pocket mechanism of seismic anisotropy (as opposed to olivine lattice preferred orientation associated with horizontal mantle flow), with low aspect ratio (~0.02) melt inclusions associated with dikes and veins, to ~75 km depth, interpreted as the base of a melt-infiltrated lithosphere. S-to-P receiver function analysis (Rychert et al., 2012) does not appear to constrain the Main Ethiopian Rift lithosphere-asthenosphere boundary, with no converted wave energy emanating from sub-Moho depths associated with the transition from fast wavespeed plate to slow wavespeed asthenosphere. This likely implies that the velocity gradient across the lithosphere-asthenosphere boundary is too shallow to yield measurable S-to-P conversions (e.g., Bastow et al., 2010; Lavayssière et al., 2018). Geophysical determinations of the lithosphere-asthenosphere boundary place its depth in the 50–80 km range.

3. Methods

A field excursion in 2008 recovered 77 samples from dikes, basaltic flows, scoria cones and silicic centers of the Galema range and surrounding areas (Fig. 1). After the 77 samples were cut to minimize alteration due to weathering, they were further cut into ~30 g billets, then polished to remove saw marks and cleaned in an ultrasonic bath of deionized water before being crushed in a steel jaw crusher and powdered in a Bico ceramic disk mill. The powders were then fused into glass discs with a lithium tetraborate ($Li_2B_4O_7$) flux following procedures detailed elsewhere (e.g., Rooney et al., 2012b). Major element oxide abundances and loss on ignition values were determined by X-Ray fluorescence analysis on a Bruker S4 PIONEER instrument at Michigan State University (supplemental material). The discs were then analyzed in triplicate for trace elements using a Photon Machines G2 excimer laser coupled to a Thermo iCap ICP-MS following procedures detailed elsewhere (Rooney et al., 2015).

4. Geochemical results

Major element geochemistry of the Galema range volcanics reveals compositions that range from picrobasalt to rhyolite (Chiasera et al., 2018). Of the samples collected in the 2008 field excursion, 66 samples contained >3 wt% MgO and 11 contained <3 wt% MgO (Chiasera et al., 2018). Major element chemical analysis of all samples and analytical duplicates are presented in the supplementary material. Major element chemical analysis, sample petrography and clinopyroxene geochemistry have been examined in previous work, indicating fractionation of olivine, plagioclase, clinopyroxene, and minor spinel (Chiasera et al., 2018). Major element geochemistry was also performed in the previous work for the purposes of characterizing the crustal level magma plumbing system and lithospheric level processes of the Galema range (Chiasera et al., 2018), and will not be discussed further here. To minimize variance associated with fractionation, we concentrate our current analyses on samples with >3 wt% MgO. CIPW norm calculations reveal that the more primitive magmas (i.e., >6 wt% MgO) of the Galema range are silica undersaturated and mildly nephelene-normative (<3% Ne).

Trace element geochemistry of samples with >6 wt% MgO display two distinct groupings when plotted on an incompatible trace element abundance diagram (Fig. 2). The first group displays an enrichment in the most incompatible trace elements with a negative K anomaly and positive Ti anomaly (Fig. 2a). The second group, exhibited by most samples from the Galema range, displays a general enrichment over primitive mantle in the most incompatible trace elements with a positive Ba anomaly, negative Th-U anomaly, and positive Nb-Ta anomaly (Fig. 2b). The Ba and Nb enrichments, relative to Th-U, and low Rb, may be due to the presence of amphibole within the source melts (e.g., Nelson et al., 2019; Rooney et al., 2014). While generally similar across samples, the relative abundance of Th to U in this group alternate, which may indicate the presence of garnet pyroxenite veins in some of the sources of the Galema range (e.g., Hirschmann and Stolper, 1996; Le Roux et al., 2011). Ti content of the different groups is most likely buffered by the presence of spinel in the source.

Trace element geochemical patterns of samples with 3–6 wt% MgO display similar trends to the more mafic samples in that they are strongly enriched in the most incompatible elements and display a negative K anomaly for the first group (Fig. 2c) and negative Th-U anomaly and positive Nb-Ta anomaly for the second group (Fig. 2d). Variations between the trace element patterns of the more evolved and primitive samples are consistent with fractionation of typical mineral phases during magma evolution (e.g., Ti variation due to fractionation of magnetite). Due to the effects on the composition imposed by crystal fractionation, samples within this range of MgO (3–6 wt%) are not considered appropriate for examination of melting processes and will not be included in the modeling procedure discussed in this work.

An additional plot of samples from the contemporaneous Pliocene-Quaternary Akaki Magmatic Zone magmas with similar MgO concentrations (Rooney et al., 2014) reveals a similar trace element pattern to the second group of Galema samples (Fig. 2b). Akaki Magmatic Zone samples also show broad similarities in trace element vs. MgO wt% plots (Rb, Nb, Zr, Yb, Eu, La) with those of the Galema range (Fig. 3). Within the Rb vs. MgO wt% plot, the subset of Akaki Magmatic Zone samples with high Rb has been attributed to the presence of phlogopite in the source melt (Rooney et al., 2014). There is some minor variance in the Ba vs. MgO wt% and Sr vs. MgO wt% data, with the Akaki Magmatic Zone displaying a slight enrichment in the more primitive samples (Fig. 3). The differences in Ba and Sr concentration between the Akaki Magmatic Zone and Galema range may be due to differences in mineralogy within the SCLM across the region (e.g., Furman and Graham, 1999), specifically amphibole content (Rooney et al., 2014). La/Nb and Ce/Pb show no significant evidence for crustal assimilation (e.g., Furman et al., 2006a; Furman et al., 2006b; Mana et al., 2012; Rooney et al., 2005; Rooney et al., 2007) (Fig. 4). The broad parallels between the compositions of the Galema range and the Akaki Magmatic Zone indicate similarity in magmatic processes between the two locations.

Magmas from the first group of the Galema range display characteristics similar to those identified as basanites from the Miocene volcano Gerba Guracha on the northwestern Ethiopian plateau (Rooney et al., 2017b). Specifically, both magma suites display primitive mantle-normalized trace element patterns of elevated Nb and Ta but lack the

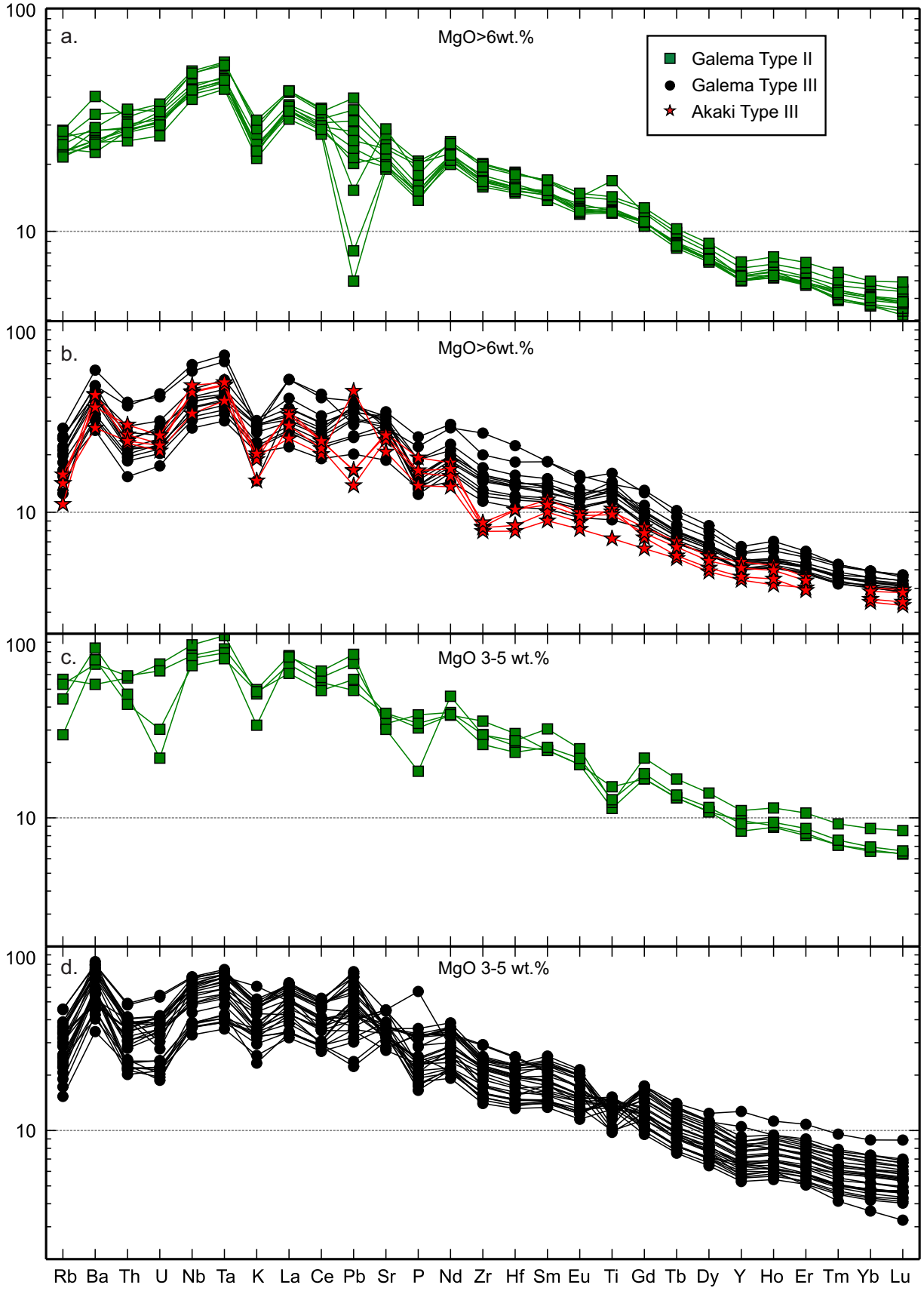

Fig. 2. Primitive mantle (MORB (Sun and McDonough, 1989)) normalized trace element diagrams for Galema range and Akaki Magmatic Zone samples with greater than 6 wt% MgO (a, b) and 3–6 wt% MgO (c, d). Akaki Magmatic Zone data are from Rooney et al. (2014).

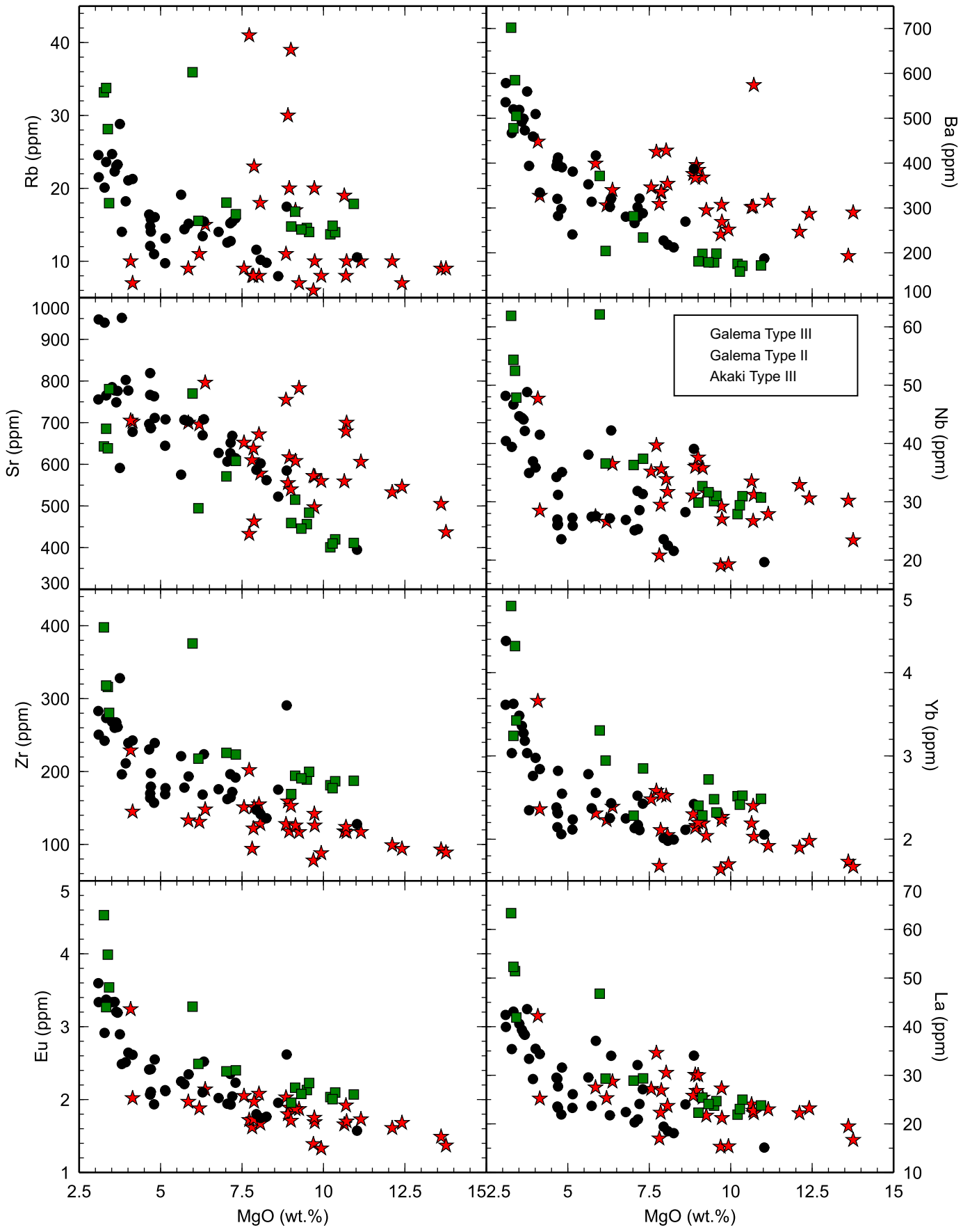

Fig. 3. Bivariate plot for samples from the Galema range and Akaki Magmatic Zone for samples with >3 MgO wt%. Symbols are the same as Fig. 2. Akaki Magmatic Zone data are from Rooney et al. (2014).

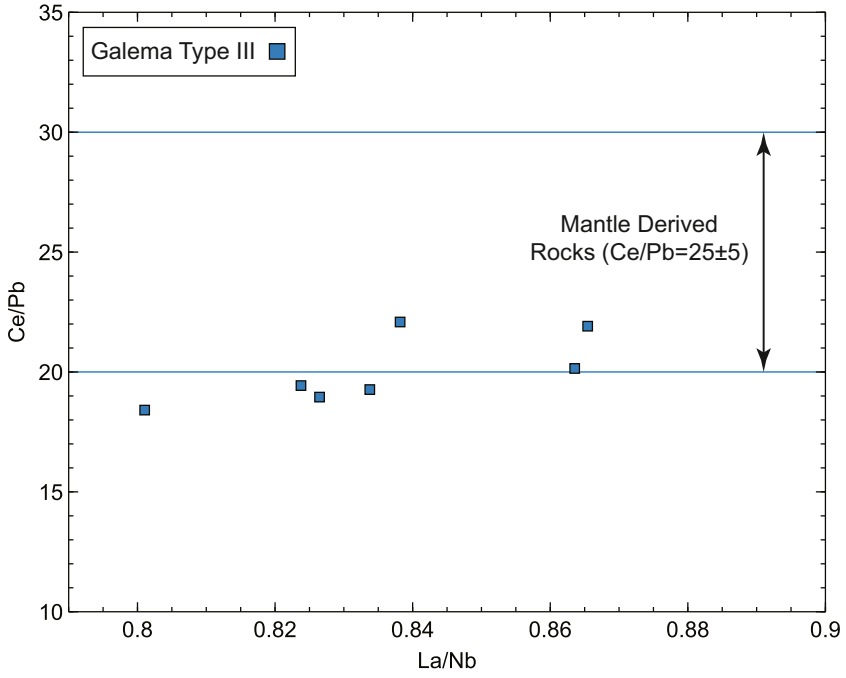

Fig. 4. Galema Type III samples plotted on Ce/Pb vs. La/Nb diagram indicating little to no crustal assimilation. The Ce/Pb value range of mantle derived rocks of 25 ± 5 from Hofmann et al. (1986).

strong positive Ba anomaly common in many Ethiopian basalts (Rooney, 2017). Examination of the geochemistry of the basanites from Gerba Guracha led to the interpretation that they were the result of melts derived from a mixture of asthenospheric and metasomatized lithospheric mantle sources (Rooney et al., 2017b). We assume a similar origin for the Galema Range lavas that display parallel geochemical characteristics. While previous work modeled the evolution and magma plumbing system of these magmas (Chiasera et al., 2018), modeling of the asthenospheric melting conditions for these lavas has not yet been performed. Existing thermo-barometric models typically presume standard peridotite source lithologies, creating significant complexity for any forward or inverse models of melt generation from the metasomatic-influenced lithospheric mantle, and this group will not be modeled in the current work.

Primitive mantle-normalized diagrams of the second group of magmas of the Galema range display characteristics similar to those identified in the Type III group of magmas of the East African Rift (Fig. 2b, d) (Rooney, 2017). This trace element geochemistry pattern is widely distributed in Cenozoic magmas and is found in locales across East Africa and is interpreted to have formed from a mixture of the Afar plume, depleted upper mantle peridotite, and a lithospheric component (Alene et al., 2017; Barrat et al., 1998; Deniel et al., 1994; Feyissa et al., 2017; Furman et al., 2006a; Hart et al., 1989; Nelson et al., 2019; Rooney, 2020c; Rooney et al., 2012a; Schilling et al., 1992), and provide an opportunity to constrain the conditions of melt generation. Mafic samples of the Akaki Magmatic Zone (>6 wt% MgO) (Rooney et al., 2014) also display similar trace element geochemistry to the Type III magmas of the East African Rift System (Fig. 2b). To determine melting conditions of the magmas of the Galema range, only primitive samples with >6 wt% MgO were considered for modeling.

The magmatic sources of the Akaki Magmatic Zone have been determined through trace element geochemical modeling to be a mixture of Afar plume, depleted mantle and Pan-African lithosphere lithologies (Rooney et al., 2014), similar to other areas of magmatism within the East African Rift System (Alene et al., 2017; Feyissa et al., 2017; Furman et al., 2006a; Rooney, 2020c; Rooney et al., 2012a). As the contemporaneous Akaki Magmatic Zone lies on the conjugate rift margin from the Galema range, and its trace element geochemistry shows striking similarities to Galema range samples (Fig. 2), it is a logical assumption that magmatic processes in the two areas may have been similar. Thus, we use the previous interpretations of the Akaki Magmatic Zone melting parameters for comparison to our determinations for the Galema range.

5. Geochemical model parameters

The similarities of the plots of the trace element geochemistry of Galema range primitive magmas (Fig. 2) to the magma groups of Rooney (2020b) suggest that the source of their parental melts was a mixture of a lithospheric component, depleted mantle, and Afar plume. The contribution from the Afar plume is likely responsible for the elevated mantle potential temperatures (T_P) found throughout the region (e.g., Ferguson et al., 2013; Rooney et al., 2012c). To determine if the Galema melts were generated in response to increased T_P, and how the multiple melt lithologies were derived and combined to create the Galema melt composition, we first examined the depth and temperature at which the melt equilibrated with the asthenosphere (T) before intrusion into the lithosphere. Models that employ major element geochemistry effectively probe the conditions under which a magma last equilibrated with the asthenosphere (Herzberg and O'Hara, 2002; Kimura and Ariskin, 2014; Kimura and Kawabata, 2014; Lee et al., 2009). This could be the result of extraction of an equilibrated melt from its solid residual, or a melt that has fully re-equilibrated with the surrounding asthenosphere on ascent, or it may reflect the average pressure and temperature conditions of fractional melts that have stalled on ascent. The Si-Mg thermobarometric model of Lee et al. (2009) was used after correction to primary compositions using the Petrolog v.3.1.1.3 modeling suite (Danyushevsky and Plechov, 2011).

The conditions of melt generation were examined using trace element thermodynamic modeling to determine how the thermochemical anomaly of the Afar plume impacted formation of the Galema magmas. Models that determine the evolution of trace element geochemistry of a magma reveal information about conditions of initial magma generation (Kimura and Kawabata, 2014; McKenzie and O'Nions, 1991). The Hydrous Adiabatic Melting Model Simulator version 1 (HAMMS1) modeling suite (Kimura and Kawabata, 2014) was used to

determine the pressures and mantle potential temperatures (T_P) at which the Galema melts were generated. For comparison, the ambient mantle temperature (T) determined by the major element thermobarometer was corrected to mantle T_p following the conversion of Katz et al. (2003). Here we explore the utility of the magma generation and evolution as probes of the rifting process, specifically the extent to which the lithosphere has been thinned.

5.1. Conditions of melt equilibration

To determine whether the ambient mantle temperature (T) was sufficiently elevated to generate the Galema range magmas, the Si-Mg thermobarometer of Lee et al. (2009) was employed, which determines equilibrium conditions of a primary magma that has not yet undergone significant fractionation. SiO_2 is buffered at given temperatures and pressures by the mineralogy of the system, and it is not greatly affected by source composition (Lee et al., 2009). This thermobarometer requires that a magma be corrected to primary compositions (Fo content = 0.90). Primary compositions thus should be unaffected by crystal phase fractionation during magmatic evolution and are equivalent to the composition of the magma when it was last in equilibrium with the mantle (Lee et al., 2009). The Galema range basalts display the presence of both olivine and plagioclase in the more primitive samples (Chiasera et al., 2018), indicating that both phases must be corrected for to achieve primary melt compositions. As the model of Lee et al. (2009) only corrects to primary compositions for olivine fractionation, the Galema basalt compositions were first back-corrected to primary melt composition for plagioclase, olivine, and clinopyroxene fractionation using the reverse fractional crystallization component of the Petrolog v.3.1.1.3 modeling suite (Danyushevsky and Plechov, 2011) (Fig. 5), following the methodology described in El-Rus and Rooney (2017). Details can be found in the supplemental material.

Initial pressure (0.7 GPa) and fO_2 values (QFM + 0.16) for the back-correction calculations were taken from Chiasera et al. (2018). Samples 3030, 3031, 3042, 3061, 3063 and 3077 (supplemental material) were chosen from the Group III Galema magmas based on their minimal modal abundance of plagioclase (Chiasera et al., 2018), which yielded successfully-corrected primary melt compositions, as detailed in the supplemental material. These back-corrected compositions were then used as thermobarometer inputs, effectively bypassing the built-in back-correction procedure for the Lee et al. (2009) model. Akaki Magmatic Zone samples 2001, 2004, 2006 and 2029 (supplemental material) were also chosen for the same thermobarometric calculations based on MgO concentration (>6 wt%) and lack of plagioclase phenocrysts. The Akaki Magmatic Zone samples did not require correction to primary compositions on the basis of plagioclase fractionation, and thus the built-in olivine correction of Lee et al. (2009) was utilized.

After correcting to primary melt compositions, the results of the thermobarometry calculations from the Lee et al. (2009) model for the Galema samples indicate temperatures of 1435–1471 °C and pressures of 2.1–2.6 ± 0.2 GPa (supplemental material). The results of the thermobarometry calculations from the Lee et al. (2009) model for the Akaki Magmatic Zone samples similarly indicate a temperature range of 1416–1452 °C and pressure range of 2.1–2.5 ± 0.2 GPa for magma equilibrium (supplemental material). These results differ from previous major element geochemical modeling within Excel MELTS (Asimow and Ghiorso, 1998; Ghiorso and Sack, 1995; Gualda and Ghiorso, 2015), which suggested two magma storage pressures; ~7 and ~ 3 kbar (Chiasera et al., 2018). The differences between the two major element models illustrate the pressures derived from the Lee et al., 2009 model are representative of magma re-equilibration with the asthenosphere, while the lower pressures derived from Excel MELTS indicate depths of magma stalling and fractionation within the lithosphere.

The following conversion for pressure (p) to depth (h) was utilized:

$$p(h) = \rho g h,$$

in which $p(h)$ = pressure in Pa, ρ = mean density of the crust/mantle column (2900 kg/m^3; Dziewonski and Anderson, 1981), g = gravitational acceleration (9.81 m/s^2), and h = depth in meters. From this equation the approximate depth range for the Galema range samples is 74–91 ± 7 km. The approximate range of depths for the Akaki Magmatic Zone samples is 74–88 ± 7 km. Models that employ major element geochemistry are useful in the determination of equilibrium conditions of a magma (Herzberg and O'Hara, 2002; Kimura and Ariskin, 2014; Kimura and Kawabata, 2014; Lee et al., 2009). As such, these results reflect depths at which the Galema magmas last equilibrated with the asthenosphere, prior to intrusion into the lithosphere (Lee et al., 2009). We interpret these depths to be those of the lithosphere-asthenosphere boundary (lithosphere-asthenosphere boundary), which represents a barrier to magma ascent (Havlin et al., 2013).

The back-corrected compositions of the Galema range basalts were also applied to the major element, MgO-T thermobarometer of HAMMS1 (Herzberg and O'Hara, 2002; Kimura and Kawabata, 2014). The temperature, pressure and melt fraction values from the MgO-T thermobarometer in HAMMS1 are estimates of the conditions of final equilibration of the melt with mantle (Herzberg and O'Hara, 2002; Kimura and Kawabata, 2014). The results of the HAMMS1 model indicate a temperature range of 1430–1474 °C, a pressure range of 2.2–2.6 GPa, and a melt fraction (F%) range of 9–11% for the Galema range basalts (supplemental material). The approximate range of equivalent depths of these pressures is 77–91 km (Fig. 7). For the Akaki Magmatic Zone samples, the major element, MgO-T thermobarometer of HAMMS1 indicates a temperature range of 1400–1434 °C, a pressure range of 2.3–2.5 GPa, and a melt fraction range of 4–6% (supplemental material). The approximate range of equivalent depths for these pressures is 81–88 km (Fig. 7).

To convert the temperatures calculated from the major element thermobarometer of Lee et al. (2009) to mantle T_P, we use the correction from T to T_P of Katz et al. (2003) combined with the potential temperature calculations of Putirka et al. (2007). Initial results of this conversion using the input parameters of Katz et al. (2003) were up to ~70 °C above the T_P values returned from the HAMMS1 trace element modeling (see Section 5.2). However, the input parameters used in Katz et al. (2003) of 0.16 for modal cpx % (wt%) and 3.3 × 10^3 kg m^{-3} for ρ_s (density of the solid) are based on values for spinel lherzolite (Katz et al., 2003). The HAMMS1 modeling of our sample compositions identifies pressures of melting greater than 2.9 GPa (~101 km). At depths greater than ~90 km, this composition should be within the garnet/spinel transition zone. Thus, input parameters may be more variable and perhaps should represent either a spinel lherzolite, garnet lherzolite, or properties intermediate to these compositions. Using input parameters for a garnet lherzolite of 3.35 × 10^3 kg m^{-3} for ρ_s and 0.02 for modal cpx % (Maaløe and Aoki, 1977) within the Katz et al. (2003) conversion results in T_P values that more closely match those determined from the HAMMS1 trace element model (Fig. 7) (supplemental material). The conversion calculations result in an average adiabat of 21 °C/GPa at 1430 °C (Fig. 7), similar to the 20 °C/GPa derived by McKenzie and Bickle (1988) for the upper mantle and the 18 K/GPa at 1500 °C derived by Katz et al. (2003). The large variance in T_P may arise from unknowns in the water saturation curve at pressures greater than 2 GPa (Katz et al., 2003).

5.2. Conditions of melt generation

Trace element geochemical models can help constrain the initial conditions of melt generation (e.g., Kimura and Kawabata, 2014; McKenzie and O'Nions, 1991). To determine the temperatures and pressures of melt generation for the Galema range basalts, the HAMMS1 model of Kimura and Kawabata (2014) was used. HAMMS1 estimates the temperature, pressure, water content, melt fraction and contamination percentage of a magma through iterative forward modeling of melt composition(s). The primary method of estimation is based on

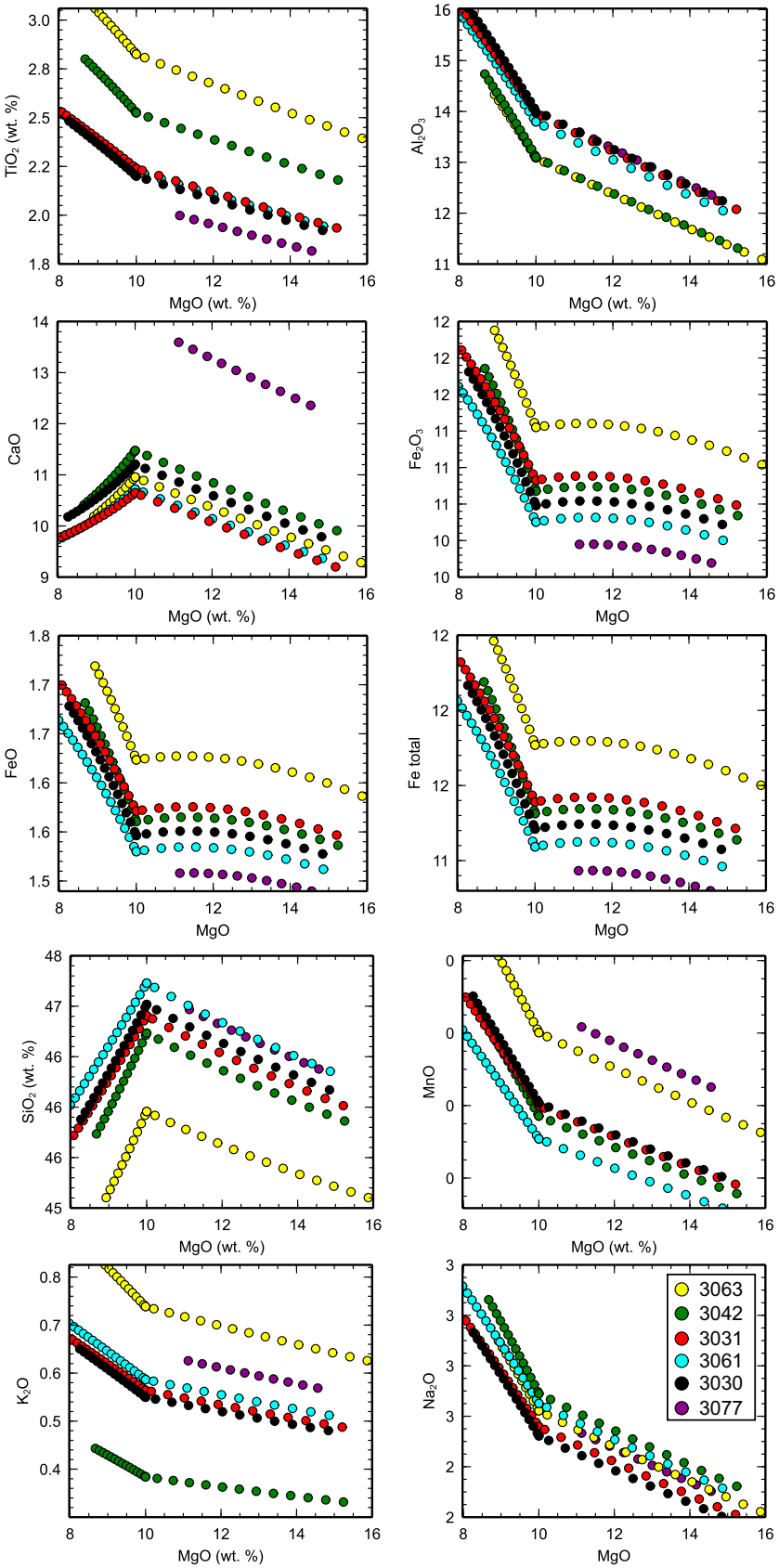

Fig. 5. Bivariate plot showing vectors of major element compositions during back correction for olivine and clinopyroxene. Back corrections performed using Petrolog v. 3.1.1.3.(Danyushevsky and Plechov, 2011).

fitting predicted concentrations of trace elements, after application of intensive variables to melting calculations, with those of the measured magma. As trace elements are particularly sensitive to processes of melting (Kimura and Kawabata, 2014; McKenzie and O'Nions, 1991), this modeling methodology is useful in determining the primary intensive parameters of magma generation. However, as HAMMS1 employs a forward modeling approach, prior knowledge of the initial source lithology and composition is necessary, which will be estimated in the following section using previous work in the region.

As noted previously, most Galema range basalts follow a pattern of a Type III magma, which is interpreted to be the result of a mixing of three source reservoirs: depleted upper mantle (DM), Afar plume (AP), and a lithospheric component (sub-continental lithospheric mantle), similar in composition to other areas of the Main Ethiopian Rift (Alene et al., 2017; Feyissa et al., 2017; Furman et al., 2006a; Rooney, 2020c; Rooney et al., 2012a). The relative concentrations of these components in the source of magmas from the central Main Ethiopian Rift have been estimated as ~80% depleted upper mantle (DM), ~20% Afar plume (AP), and small amounts of a lithospheric component. The lithospheric component was likely a portion of the lower sub-continental lithospheric mantle (SCLM) that foundered (e.g., Bédard, 2006; Lee et al., 2011; Van Wijk et al., 2008) and mixed into the depleted upper mantle as a result of thermal/chemical erosion by the Afar plume (Furman et al., 2016; Rooney et al., 2012a). Thus, we have chosen an 80:20 (DM:AP) mixture as our starting

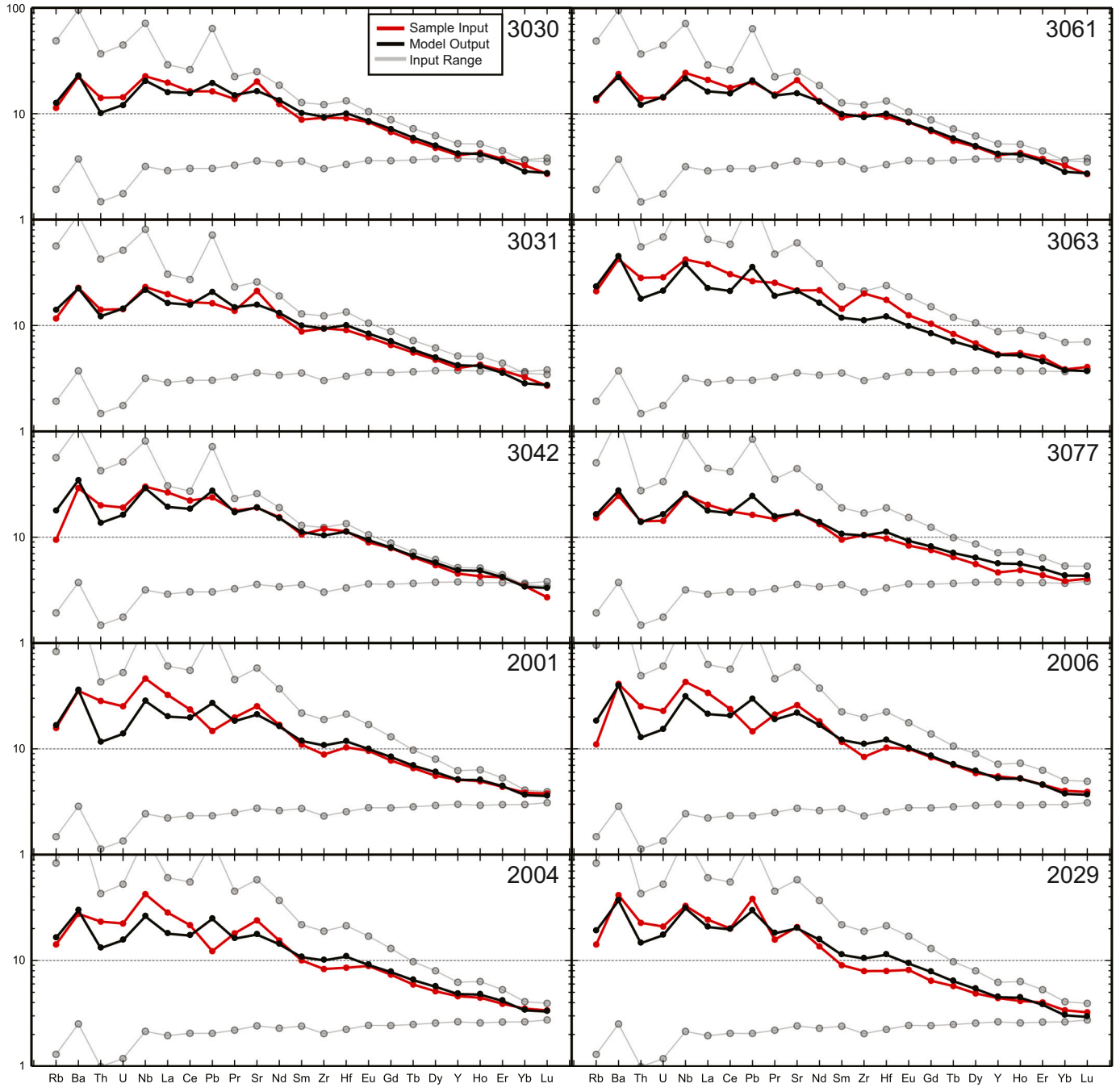

Fig. 6. Trace element spider diagrams showing selected samples input into to the HAMMS modeling suite (Kimura and Kawabata, 2014) for selected Galema range and Akaki Magmatic Zone samples. See text for discussion on source chemistry and mantle conditions used. Akaki Magmatic Zone data from Rooney et al. (2014). Light grey plots represent model outputs for the end member values of the range of initial conditions described in the main text (1500 °C, 2GPa, 1% lithosphere for the enriched plot and 1411 °C, 3GPa, 1% lithosphere for the depleted plot).

melt lithology for the HAMMS1 calculations (supplemental material). All Galema range samples with >6.0 wt% MgO display values of Ni/Co < 4 and Co/Fe < 7, placing them within fields for an eclogite source, as described by Le Roux et al. (2011). To account for the lithospheric component we have chosen a composition equal to an experimental analysis of melting of a clinopyroxenite-hornblendite (Pilet et al., 2008) (supplemental material). As we have determined that there is little to no crustal contamination of the Galema samples, the chemistry of crustal material built-in to HAMMS1 as a contaminant was not used. Instead, the lithospheric composition was entered into HAMMS1 in place of the built-in chemistry of crustal material in order to vary its concentration during processing. For continuity of process, we used the same Galema Type III and Akaki Magmatic Zone samples that were used for the Lee et al. (2009) thermobarometer analysis discussed above (supplemental material).

Within the HAMMS1 model, the temperature, pressure, H_2O content, and contamination percentage were all varied systematically within specified ranges (temperature: 1300–1500 °C, pressure: 3.5–2.0 GPa., H_2O: 0–1 wt%, lithospheric component: 0–5%) to achieve an acceptable match between the trace element concentrations of the modeled melt and the Galema range basalt composition. In addition to the trace element calculations, melting pressures and temperatures determined from MgO melt thermometry (Herzberg and O'Hara, 2002; Kimura and Ariskin, 2014) and melt fraction (F%) for a peridotite source were also calculated within HAMMS1 for selected samples (Kimura and Kawabata, 2014).

The conditions of the HAMMS1 calculations that best matched the trace element distribution of the observed data for the magmas of the Galema range are 1418–1450 °C at a pressure range of 2.9–3.2 GPa under anhydrous conditions, with lithospheric component additions of 0.5–1.1% (Fig. 6) (supplemental material). The input conditions that best fit the observed data for the Akaki Magmatic Zone samples have a similar temperature and pressure range (1430–1438 °C; 3.0–3.1 GPa), with lithospheric component additions of 0.8–1.5% (Fig. 6) (supplemental material). This results in an estimated melt generation depth range of 102–112 km for the Galema range, and 105–109 km for the Akaki Magmatic Zone samples (Fig. 7).

Source mineralogy for both the Galema range and Akaki Magmatic Zone samples was also calculated by HAMMS1 for the indicated melting pressures. The Galema range melts display an average mineral composition of 59 wt% olivine, 2 wt% garnet, 17 wt% opx, and 21 wt% cpx (supplemental material). The Akaki Magmatic Zone melts display an average mineral composition of 60 wt% olivine, 2 wt% garnet, 18 wt% opx, and 21 wt% cpx (supplemental material). The HAMMS1 model does not include spinel in these calculations due to low partition coefficients for most incompatible trace elements (Kimura and Kawabata, 2014).

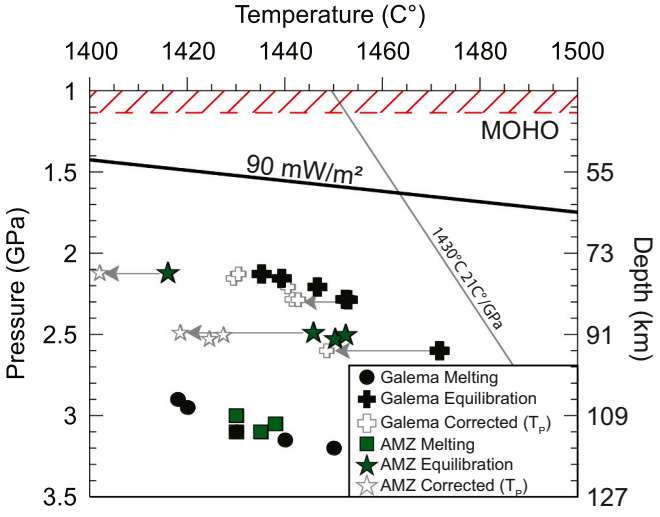

Fig. 7. Pressure temperature chart of melting and asthenospheric equilibration of the Galema range and Akaki Magmatic Zone Type III magmas. Temperature and pressure estimates from our thermodynamic, trace element modeling (HAMMS1) (Kimura and Kawabata, 2014) and major element, olivine thermobarometry (Lee et al., 2009). Moho depth estimates from Keranen et al. (2009). Geotherm estimate from Hasterok and Chapman (2011).

6. Discussion

6.1. East African upper mantle T_P during the Pliocene-Quaternary transition

The results of the SiO_2 thermobarometry indicate that the temperature (T) during the final equilibration with the mantle of the Galema range magmas (1435–1471 °C), as well as the contemporaneous Akaki Magmatic Zone (1416–1452 °C), were broadly equivalent, even though they occur on opposite sides of the rift. The mantle temperature (T) derived from the major element thermobarometry of HAMMS1 indicates a similar range of melt equilibrium temperatures for the magmas of the Galema range (1430–1474 °C) and the Akaki Magmatic Zone (1400–1434 °C). The results of the HAMMS1 trace element model indicate mantle potential temperature (T_P) for the initial melting of the Galema range magmas is similar as well, 1418–1450 °C. The temperatures from the HAMMS1 model (T and T_P) display remarkable coherence with the independently-derived, corrected temperatures of the SiO_2 thermobarometry, indicating elevated mantle temperatures regardless of whether they are T_P or temperatures of equilibration.

Our estimates for elevated T_P in the East African upper mantle during the Pliocene-Quaternary are consistent with other estimates for the region. For example, magmatic volume estimations from the Virunga province indicates that a mantle $T_P \approx 1430$ °C is necessary for the southern East African Rift System during the Quaternary (Rogers et al., 1998). Beccaluva et al. (2009) used the petrogenetic modeling techniques of Albarede (1992) to determine mantle $T_P = 1200–1500$ °C for Eocene Ethiopian flood basalts on the northwestern Ethiopian plateau. Thermodynamic calculations (PRIMELT-2; Herzberg and Asimow, 2008) performed on a large dataset from East Africa have shown that mantle T_P of the East African Rift System was at its highest, ~170 °C above the ambient T_P of 1350 ± 50 °C, during the Oligocene, but has subsequently cooled to the current state of ~140 °C above ambient (Rooney et al., 2012c). The Si-Mg thermobarometer of Lee et al. (2009) has previously been applied to Quaternary magmas from Afar, resulting in a T_P range of 1472–1489 °C (Ferguson et al., 2013). REE inversion modeling (McKenzie and O'Nions, 1991) was also applied to these Quaternary Afar magmas, resulting in a T_P estimate of 1450 °C (Ferguson et al., 2013). When combined with our thermobarometry calculations, it is apparent that there is a growing consensus that the mantle T_P of East Africa is elevated above that of ambient upper mantle and it has been this way since at least the Eocene.

A consensus has emerged amongst the seismological community that the Ethiopian mantle is characterized by markedly deep-seated (e.g., Benoit et al., 2006a; Benoit et al., 2006b; Boyce et al., 2021; Chang and Van der Lee, 2011), high amplitude (e.g., Bastow et al., 2008; Bastow et al., 2010; Boyce et al., 2021; Gallacher et al., 2016), slow wavespeed anomalies. The Ethiopian upper mantle is, in fact, seismically amongst the slowest worldwide (Bastow, 2012), completely inconsistent with a decompression melting of ambient mantle. Our observations of relatively deep mantle melting at elevated T_P below Ethiopia corroborate these studies and emphasize the requirement for both elevated temperatures and mantle melting to explain the seismic observations.

6.2. Depth of the lithosphere-asthenosphere boundary during the Pliocene-Quaternary transition

Broad constraints on lithosphere-asthenosphere boundary depth can

be gained by examining mantle xenoliths and depth of melt generation – such data provide limits as to the range of pressures where the lithosphere-asthenosphere boundary may occur. Using these broad constraints, we examined the depth range possible for the lithosphere-asthenosphere boundary in the northern EAR and explored melt equilibration pressures as a proxy for lithosphere-asthenosphere boundary depth.

6.2.1. Constraints on the extent of the continental lithospheric mantle

Xenolith thermobarometry studies performed on peridotite and pyroxenite xenoliths throughout the Main Ethiopian Rift have determined equilibration pressures that extend to 1.4 GPa (~49 km depth) (Alemayehu et al., 2017; Conticelli et al., 1999; Ferrando et al., 2008; Rooney et al., 2005; Rooney et al., 2017a; Trestrail et al., 2017). Xenolith suites rarely sample the lithosphere-asthenosphere boundary, so these calculations represent a minimum thickness of the continental lithosphere at the time of eruption.

Constraining the depth of melt generation for rift lavas provides an indirect probe of the thickness of the continental lithospheric mantle; the base of the lithospheric mantle must be shallower than the melting column. Existing estimates of the melt generation depth of magmas in the region are focused upon Quaternary lavas, providing insight into the current state of mantle melting. REE inversion modeling (McKenzie and O'Nions, 1991) was applied to Afar magmas, resulting in a depth estimate of the melting column to be 80–95 km (Ferguson et al., 2013). These estimates of the depth of the melting column in Afar, combined with estimates of extension rates, have led to the interpretation that the lithosphere in the area is 60–80 km thick (Ferguson et al., 2013). Quaternary magmas from the northern Main Ethiopian Rift have an estimated melting depth range of 53–100 km, with the shallower depth interpreted as the base of the lithosphere northern Main Ethiopia Rift (Ayalew and Gibson, 2009; Furman et al., 2006b; Rooney et al., 2005).

Our new results from the Pliocene-Quaternary Galema range basalts are broadly parallel to the Quaternary studies results with pressure ranging from 2.1 to 3.2 GPa (74–112 km). However, this large range in values obscures some consistent deviations in estimates of melt pressures and temperatures that may arise from the methodology used, which effectively probes two different processes: melt generation, derived from trace element geochemistry (Kimura and Kawabata, 2014; McKenzie and O'Nions, 1991), and melt equilibration within the asthenosphere, derived from major element geochemistry (Herzberg and O'Hara, 2002; Kimura and Ariskin, 2014; Kimura and Kawabata, 2014; Lee et al., 2009). Estimates of melting depth that are based on trace element geochemistry reveal information pertaining to the depth of initial melt generation (Kimura and Kawabata, 2014; McKenzie and O'Nions, 1991). The HAMMS1 trace element modeling results suggest melt generation pressures for the Galema range to be 2.9–3.2 GPa (102–112 km depth) and 3–3.1 GPa (105–109 km depth) for the contemporaneous Akaki Magmatic Zone.

Depth estimates based on major element geochemistry reveal the pressures at which the melt last equilibrated (e.g. stalled) within the asthenosphere, before intrusion into the lithosphere (Herzberg and O'Hara, 2002; Kimura and Ariskin, 2014; Kimura and Kawabata, 2014; Lee et al., 2009). Our SiO_2 thermobarometry calculations show the magmas of the Galema range re-equilibrated with the asthenosphere at pressures of 2.1–2.6 ± 0.2 GPa (~74–91 km depth), and Akaki Magmatic Zone magmas have comparable values at 74–88 km. The results of the major element thermobarometry estimates from HAMMS1 suggest similar pressure-temperature conditions: the Galema range is 2.2–2.6 GPa (77–91 km depth), while the Akaki Magmatic Zone is 2.3–2.5 GPa (81–88 km depth).

We have demonstrated that a consistent deviation exists between the depth of melt generation (102–112 km) and depth of re-equilibration (~74–91 km) for the Galema range. We have also demonstrated a similar deviation for the depth of melt generation (105–109 km) and melt re-equilibration (~81–88 km) for the Akaki Magmatic Zone. The results of our thermo-barometric modeling of magmatism on both rift margins (Galema range and Akaki Magmatic Zone) show an anomalously high mantle T_P (+ ~ 68–100 °C) and a melt stalling/re-equilibration depth of ~80 km, interpreted as the lithosphere-asthenosphere boundary. Next, we explore how this model correlates with the existing geophysical literature.

6.2.2. Implications for geophysical constraints on plate thickness

The P-wave velocity model of Bastow et al. (2008) reveals slow uppermost mantle wavespeeds beneath the Galema range (Fig. 8). Vertical smearing of anomalies is always a feature of teleseismic body-wave travel-time tomography studies such as Bastow et al. (2008), but the depth-extent of slow wavespeeds below Galema is consistent with an ~80 km thick lithospheric layer. The slow-wavespeed anomaly amplitudes below Galema are markedly lower than below the Main Ethiopian Rift to the west, attesting to a zone of past melt intrusion which is still at higher temperatures than that of adjacent Somali Plate lithosphere.

S-to-P receiver functions are a common tool for detecting the base of the lithosphere via detection of the boundary between fast wavespeed lithosphere and slower underlying asthenosphere. However, detection of such a boundary below the Main Ethiopian Rift has been controversial. Rychert et al. (2012) interpreted a negative polarity signal at ~75 km depth below the Main Ethiopian Rift as the onset of decompression melting of ambient mantle below a plate with no lithospheric mantle. The T_P anomaly estimates we obtained in this work (up to 100 °C), when reviewed in light of Ethiopia's markedly deep-seated slow wavespeeds (e.g., Bastow et al., 2008; Boyce et al., 2021; Gallacher et al., 2016), render the ambient mantle decompression melting hypothesis implausible. Further, the occurrence of the magmas affected by metasomatic processes (Rooney et al., 2017b) within the suite of lavas erupted within the Galema range indicates melts were derived from metasomatized lithospheric mantle, not ambient asthenosphere. Observations of seismic anisotropy below the Main Ethiopian Rift also require high aspect ratio melt intrusions to mantle lithospheric depths of ~75 km depth (e.g., Bastow et al., 2010). In any case, re-analyzing the same S-to-P dataset using near-identical techniques, Lavayssière et al. (2018) found no evidence for any sub-Moho P-to-S converted energy signal below the central Main Ethiopian Rift, in contrast to Rychert et al. (2012). The lack of a receiver function signal below both the central Main Ethiopian Rift, and the Galema range, testifies to a lithosphere whose base has been thermally altered significantly during episodes of magma intrusion; therefore, it lacks strong wavespeed contrast with the asthenosphere below. Depth constraints on shear wavespeed from surface wave studies confirm the gradational velocity profile hypothesis (e.g., Bastow et al., 2010; Dugda et al., 2007).

Our results further support present-day estimates of lithosphere-asthenosphere boundary depth below Galema from the surface wave literature (60–80 km; Dugda et al., 2007) and from the aforementioned surface wave study of seismic anisotropy by Bastow et al. (2010), which proposed a plate thickness of ~75 km for the Main Ethiopian Rift and its flanks. While wide-angle seismic profiles (Mackenzie et al., 2005; Maguire et al., 2006) do not penetrate the entire lithosphere, they do resolve a 55–60 km-deep mantle reflector – the 'L' reflector. Our inferred ~80 km estimate for lithosphere-asthenosphere boundary depth corroborates the conclusion of Maguire et al. (2006) that the L-reflector is not the lithosphere-asthenosphere boundary, but is instead a mid-lithosphere discontinuity. The results of our study therefore clarify the existing geophysical observations on the depth of Ethiopian lithosphere-asthenosphere boundary, for which consensus has been lacking. When reviewed in light of geophysical constraints, our work supports the view that magmatic extension during rift development can commence while the plate remains thick, and magmatism is not necessarily an immediate precursor to seafloor spreading in a new ocean basin.

6.2.3. Hybrid source generation and lithospheric removal

Combined with existing isotopic constraints (Rooney et al., 2012a),

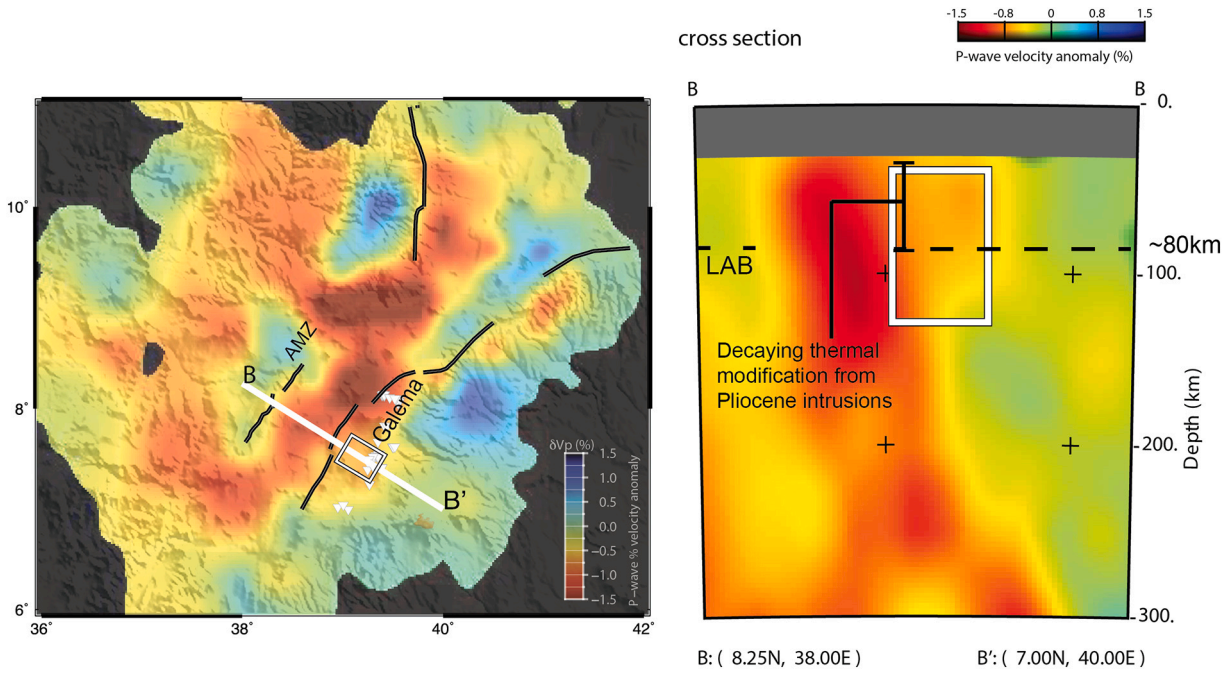

Fig. 8. 75 km depth-slice through the P-wave velocity model of (Bastow et al., 2008) and associated cross section (B-B′) for orthogonal transect across the Galema range. Areas of poor ray coverage are black. Heavy black lines are major Miocene border faults. Triangles are our sample locations. The grey band at the top of the cross-section masks anomalies that are not resolved by the inversion scheme.

our new trace element modeling requires that, prior to the commencement of magmatic activity within the modern Main Ethiopian Rift, lithospheric material foundered and mixed with the ambient asthenosphere (e.g., Furman et al., 2016; Rooney et al., 2012a). Increased mantle T_P, as a result of the impingement of the Afar plume (e.g., Beccaluva et al., 2009; Ferguson et al., 2013; Rogers et al., 1998; Rooney et al., 2012c), generated melts of both the plume and hybrid ambient upper mantle that mixed to form Type III magmas (e.g., Furman et al., 2006a; Rooney et al., 2012a; Rooney et al., 2013; Schilling et al., 1992). The resultant magmas ascended and stalled at the LAB, allowing for partial re-equilibration with the surrounding mantle. As these magmas intruded the lithosphere, they raised the temperature of the SCLM and initiated melting of metasomatic veins – creating Type II magmas.

6.2.4. *Magmatically assisted continental rifting*

Our results place rift-adjacent areas of focused magmatism, such as the Galema range and Akaki Magmatic Zone, within the broader context of the rifting processes affecting the East African Rift System. Previous studies have suggested that magmatism occurs after the formation of, and within the confines of, rift border faults (Ebinger and Casey, 2001; Hayward and Ebinger, 1996; Wolfenden et al., 2005). Our results further support the results of Chiasera et al. (2018) that focused magmatic intrusion associated with continental rifting may occur over a broader area, including outside of the rift-border faults. Magmatic intrusion is necessary to thermally weaken the lithosphere to allow rifting to proceed (Bialas et al., 2010; Buck, 2006). The bulk of this magmatism is attributed to adiabatic melting associated with lithospheric thinning and ascent of the underlying asthenosphere (Bastow et al., 2008; Bastow and Keir, 2011; Yirgu et al., 2006). Lithospheric thinning is attributed to stretching of the lithosphere during extension (e.g., White and McKenzie, 1989) and thermomechanical erosion of the SCLM by the impingement of the Afar plume (e.g., Davies, 1994; Furman et al., 2016; Spohn and Schubert, 1982).

7. Conclusions

The melts of both the Galema range and the contemporaneous Akaki Magmatic Zone along the western rift flank were generated as a result of an increased T_p of ~1450 °C (~100 °C above ambient mantle). Our thermodynamic modeling and thermobarometric calculations indicate that the melts ascended from their depth of generation at ~110 km to stall at ~80 km depth where they partially re-equilibrated at the base of the plate. P-wave tomographic models reveal a low velocity body of material beneath the Galema range to similar depths, consistent with our hypothesis of a thermally-perturbed SCLM resulting from thermal input by the intrusion of the Galema magmas on ascent, composed of lithologies representing the Afar plume, ambient upper mantle, and metasomatized SCLM.

Our results show that the transition from mechanical plate stretching and thinning to extension via magma intrusion in the central Main Ethiopian Rift was underway in Pliocene times (~2–3 Ma) when the lithosphere remained relatively thick. Therefore, a significant proportion of decompression melting can plausibly be attributed to plate thinning in the latest stages of breakup.

Declaration of Competing Interest

None of the authors have any declaration of interest.

Acknowledgements

This work was supported by The National Aeronautics and Space Administration Planetary Geology and Geophysics Program [Grant: 10-PGG10-006]. I. Bastow acknowledges support from Natural Environment Research Council grant number NE/S014136/1. We thank Dr. Eric Brown for his assistance with the creation of this work. We thank Francesco Mazzarini and an anonymous reviewer for insightful comments that improved the manuscript. We would also like to thank journal editor Micheal Roden and journal managers Parthiban Rajendran and Shruti Venkiteswaran for their careful handling of this work.

Appendix A. Supplementary data

Supplementary data to this article can be found online at https://doi.

org/10.1016/j.lithos.2021.106494.

References

Abebe, T., Mazzarini, F., Innocenti, F., Manetti, P., 1998. The Yerer-Tullu Wellel volcanotectonic lineament: a transtensional structure in central Ethiopia and the associated magmatic activity. J. Afr. Earth Sci. 26, 135–150. https://doi.org/10.1016/S0899-5362(97)00141-3.

Abebe, T., Manetti, P., Bonini, M., Corti, G., Innocenti, F., Mazzarini, F., Pecskay, Z., 2005. Geological map (scale 1: 200,000) of the northern Main Ethiopian Rift and its implication for the volcano-tectonic evolution of the rift. Geol. Soc. Am. Map Chart Ser. MCH094.

Albarede, F., 1992. How deep do common basaltic magmas form and differentiate? J. Geophys. Res. Solid Earth 97, 10997–11009.

Alemayehu, M., Zhang, H.-F., Sakyi, P.A., 2017. Nature and evolution of lithospheric mantle beneath the southern Ethiopian rift zone: evidence from petrology and geochemistry of mantle xenoliths. Int. J. Earth Sci. 106, 939–958.

Alene, M., Hart, W.K., Saylor, B.Z., Deino, A., Mertzman, S., Haile-Selassie, Y., Gibert, L. B., 2017. Geochemistry of Woranso–Mille Pliocene basalts from west-central Afar, Ethiopia: implications for mantle source characteristics and rift evolution. Lithos 282, 187–200.

Asimow, P.D., Ghiorso, M.S., 1998. Algorithmic modifications extending MELTS to calculate subsolidus phase relations. Am. Mineral. 83, 1127–1132. https://doi.org/10.2138/am-1998-9-1022.

Ayalew, D., Gibson, S.A., 2009. Head-to-tail transition of the Afar mantle plume: geochemical evidence from a Miocene bimodal basalt–rhyolite succession in the Ethiopian Large Igneous Province. Lithos 112, 461–476.

Ayalew, D., Jung, S., Romer, R., Garbe-Schönberg, D., 2018. Trace element systematics and Nd, Sr and Pb isotopes of Pliocene flood basalt magmas (Ethiopian rift): a case for Afar plume-lithosphere interaction. Chem. Geol. 493, 172–188.

Baker, J., Snee, L., Menzies, M., 1996. A brief Oligocene period of flood volcanism in Yemen: implications for the duration and rate of continental flood volcanism at the Afro-Arabian triple junction. Earth Planet. Sci. Lett. 138, 39–55. https://doi.org/10.1016/0012-821X(95)00229-6.

Barrat, J., Fourcade, S., Jahn, B., Cheminee, J., Capdevila, R., 1998. Isotope (Sr, Nd, Pb, O) and trace-element geochemistry of volcanics from the Erta'Ale range (Ethiopia). J. Volcanol. Geotherm. Res. 80, 85–100.

Bastow, I.D., 2012. Relative arrival-time upper-mantle tomography and the elusive background mean. Geophys. J. Int. 190, 1271–1278.

Bastow, I.D., Keir, D., 2011. The protracted development of the continent–ocean transition in Afar. Nat. Geosci. 4, 248–250. https://doi.org/10.1038/ngeo1095.

Bastow, I.D., Nyblade, A.A., Stuart, G.W., Rooney, T.O., Benoit, M.H., 2008. Upper mantle seismic structure beneath the Ethiopian hot spot: rifting at the edge of the African low-velocity anomaly. Geochem. Geophys. Geosyst. 9 https://doi.org/10.1029/2008GC002107.

Bastow, I., Pilidou, S., Kendall, J.M., Stuart, G., 2010. Melt-induced seismic anisotropy and magma assisted rifting in Ethiopia: evidence from surface waves. Geochem. Geophys. Geosyst. 11.

Beccaluva, L., Bianchini, G., Natali, C., Siena, F., 2009. Continental flood basalts and mantle plumes: a case study of the Northern Ethiopian Plateau. J. Petrol. 50, 1377–1403.

Bédard, J.H., 2006. A catalytic delamination-driven model for coupled genesis of Archaean crust and sub-continental lithospheric mantle. Geochim. Cosmochim. Acta 70, 1188–1214.

Bellieni, G., Brotzu, P., Morbidelli, L., Piccirillo, E., Traversa, G., 1986. Petrology and mineralogy of Miocene fissural volcanism of the East Kenya Plateau. Neues Jahrbuch fuer Mineralogie. Abhandlungen 154, 153–178.

Benoit, M.H., Nyblade, A.A., Owens, T.J., Stuart, G., 2006a. Mantle transition zone structure and upper mantle S velocity variations beneath Ethiopia: evidence for a broad, deep-seated thermal anomaly. Geochem. Geophys. Geosyst. 7.

Benoit, M.H., Nyblade, A.A., VanDecar, J.C., 2006b. Upper mantle P-wave speed variations beneath Ethiopia and the origin of the Afar hotspot. Geology 34, 329–332.

Bialas, R.W., Buck, W.R., Qin, R., 2010. How much magma is required to rift a continent? Earth Planet. Sci. Lett. 292, 68–78. https://doi.org/10.1016/j.epsl.2010.01.021.

Boyce, A., Bastow, I., Cottaar, S., Kounoudis, R., Guilloud De Courbeville, J., Caunt, E., Desai, S., 2021. AFRP20: new P-wavespeed model for the african mantle reveals two whole-mantle plumes below East Africa and neoproterozoic modification of the Tanzania Craton. Geochem. Geophys. Geosyst. 22 p. e2020GC009302.

Buck, W.R., 2006. The role of magma in the development of the Afro-Arabian Rift System. Geol. Soc. Lond., Spec. Publ. 259, 43–54. https://doi.org/10.1144/GSL.SP.2006.259.01.05.

Chang, S.-J., Van der Lee, S., 2011. Mantle plumes and associated flow beneath Arabia and East Africa. Earth Planet. Sci. Lett. 302, 448–454.

Chernet, T., Hart, W.K., Aronson, J.L., Walter, R.C., 1998. New age constraints on the timing of volcanism and tectonism in the northern Main Ethiopian Rift–southern Afar transition zone (Ethiopia). J. Volcanol. Geotherm. Res. 80, 267–280.

Chiasera, B., Rooney, T.O., Girard, G., Yirgu, G., Grosfils, E., Ayalew, D., Mohr, P., Zimbelman, J.R., Ramsey, M.S., 2018. Magmatically assisted off-rift extension—the case for broadly distributed strain accommodation. Geosphere 14, 1544–1563.

Conticelli, S., Sintoni, M., Abebe, T., Mazzarini, F., Manetti, P., 1999. Petrology and geochemistry of ultramafic xenoliths and host lavas from the Ethiopian Volcanic Province: an insight into the upper mantle under eastern Africa. Acta Vulcanol. 11, 143–160.

Cornwell, D.G., Mackenzie, G.D., England, R.W., Maguire, P.K.H., 2006. Northern Main Ethiopian Rift crustal structure from new high-precision gravity data. In: The Afar Volcanic Province Within the East African Rift System, p. 307.

Corti, G., Cioni, R., Franceschini, Z., Sani, F., Scaillet, S., Molin, P., Isola, I., Mazzarini, F., Brune, S., Keir, D., 2019. Aborted propagation of the Ethiopian rift caused by linkage with the Kenyan rift. Nat. Commun. 10, 1309.

Danyushevsky, L.V., Plechov, P., 2011. Petrolog3: integrated software for modeling crystallization processes. Geochem. Geophys. Geosyst. 12.

Daoud, M.A., Maury, R.C., Barrat, J.-A., Taylor, R.N., Le Gall, B., Guillou, H., Cotten, J., Rolet, J., 2010. A LREE-depleted component in the Afar plume: further evidence from Quaternary Djibouti basalts. Lithos 114, 327–336.

Daoud, M.A., Le Gall, B., Maury, R.C., Rolet, J., Huchon, P., Guillou, H., 2011. Young rift kinematics in the Tadjoura rift, western Gulf of Aden, Republic of Djibouti. Tectonics 30.

Darbyshire, F.A., Eaton, D.W., 2010. The lithospheric root beneath Hudson Bay, Canada from Rayleigh wave dispersion: no clear seismological distinction between Archean and Proterozoic mantle. Lithos 120, 144–159.

Davidson, A., Rex, D., 1980. Age of volcanism and rifting in southwestern Ethiopia. Nature 283, 657–658.

Davies, G.F., 1994. Thermomechanical erosion of the lithosphere by mantle plumes. J. Geophys. Res. Solid Earth 99, 15709–15722.

Deniel, C., Vidal, P., Coulon, C., Vellutini, P.-J., Piguet, P., 1994. Temporal evolution of mantle sources during continental rifting: the volcanism of Djibouti (Afar). J. Geophys. Res. Solid Earth 99, 2853–2869.

Dugda, M.T., Nyblade, A.A., Julia, J., 2007. Thin lithosphere beneath the Ethiopian Plateau revealed by a joint inversion of Rayleigh wave group velocities and receiver functions. J. Geophys. Res. Solid Earth 112.

Dunkley, P., Smith, M., Allen, D., Darling, W., 1993. The Geothermal Activity and Geology of the Northern Sector of the Kenya Rift Valley.

Dziewonski, A.M., Anderson, D.L., 1981. Preliminary reference Earth model. Phys. Earth Planet. Inter. 25, 297–356.

Eaton, D.W., Darbyshire, F., Evans, R.L., Grütter, H., Jones, A.G., Yuan, X., 2009. The elusive lithosphere–asthenosphere boundary (LAB) beneath cratons. Lithos 109, 1–22.

Ebinger, C., Casey, M., 2001. Continental breakup in magmatic provinces: an Ethiopian example. Geology 29, 527–530. https://doi.org/10.1111/j.1468-4004.2005.46216.x.

Ebinger, C., Yamane, T., Kelley, S., 1993. Volcanism and extension between the main Ethiopian and Gregory Rifts. In: Geoscientific Research in Northeast Africa. Balkema, Rotterdam, pp. 301–304.

Ebinger, C., Yemane, T., Harding, D., Tesfaye, S., Kelley, S., Rex, D., 2000. Rift deflection, migration, and propagation: linkage of the Ethiopian and Eastern rifts, Africa. Geol. Soc. Am. Bull. 112, 163–176.

Ebinger, C., Keir, D., Bastow, I., Whaler, K., Hammond, J.O., Ayele, A., Miller, M., Tiberi, C., Hautot, S., 2017. Crustal structure of active deformation zones in Africa: implications for global crustal processes. Tectonics 36, 3298–3332.

El-Rus, M.M.A., Rooney, T.O., 2017. Insights into the lithosphere to asthenosphere melting transition in northeast Africa: evidence from the Tertiary volcanism in middle Egypt. Chem. Geol. 455, 282–303.

Ferguson, D.J., Maclennan, J., Bastow, I., Pyle, D., Jones, S., Keir, D., Blundy, J., Plank, T., Yirgu, G., 2013. Melting during late-stage rifting in Afar is hot and deep. Nature 499, 70–73.

Ferrando, S., Frezzotti, M., Neumann, E.-R., De Astis, G., Peccerillo, A., Dereje, A., Gezahegn, Y., Teklewold, A., 2008. Composition and thermal structure of the lithosphere beneath the Ethiopian plateau: evidence from mantle xenoliths in basanites, Injibara, Lake Tana Province. Mineral. Petrol. 93, 47–78.

Feyissa, D., Shinjo, R., Kitagawa, H., Meshesha, D., Nakamura, E., 2017. Petrologic and geochemical characterization of rift-related magmatism at the northernmost Main Ethiopian Rift: implications for plume-lithosphere interaction and the evolution of rift mantle sources. Lithos 282, 240–261.

Fishwick, S., Bastow, I.D., 2011. Towards a better understanding of African topography: a review of passive-source seismic studies of the African crust and upper mantle. Geol. Soc. Lond., Spec. Publ. 357, 343–371.

Furman, T., Graham, D., 1999. Erosion of lithospheric mantle beneath the East African Rift system: geochemical evidence from the Kivu volcanic province. Lithos 48, 237–262.

Furman, T., Bryce, J., Rooney, T., Hanan, B., Yirgu, G., Ayalew, D., 2006a. Heads and tails: 30 million years of the Afar plume. Geol. Soc. Lond., Spec. Publ. 259, 95–119. https://doi.org/10.1144/GSL.SP.2006.259.01.09.

Furman, T., Kaleta, K.M., Bryce, J.G., Hanan, B.B., 2006b. Tertiary mafic lavas of Turkana, Kenya: constraints on East African plume structure and the occurrence of high-μ volcanism in Africa. J. Petrol. 47, 1221–1244.

Furman, T., Nelson, W.R., Elkins-Tanton, L.T., 2016. Evolution of the East African rift: drip magmatism, lithospheric thinning and mafic volcanism. Geochim. Cosmochim. Acta 185, 418–434.

Gallacher, R., Bastow, I., 2012. The development of magmatism along the Cameroon Volcanic Line: evidence from teleseismic receiver functions. Tectonics 31.

Gallacher, R.J., Keir, D., Harmon, N., Stuart, G., Leroy, S., Hammond, J.O., Kendall, J.-M., Ayele, A., Goitom, B., Ogubazghi, G., 2016. The initiation of segmented buoyancy-driven melting during continental breakup. Nat. Commun. 7, 13110.

George, R., Rogers, N., 2002. Plume dynamics beneath the African plate inferred from the geochemistry of the Tertiary basalts of southern Ethiopia. Contrib. Mineral. Petrol. 144, 286–304. https://doi.org/10.1007/s00410-002-0396-z.

George, R., Rogers, N., Kelley, S., 1998. Earliest magmatism in Ethiopia: evidence for two mantle plumes in one flood basalt province. Geology 26, 923–926.

Ghiorso, M.S., Sack, R.O., 1995. Chemical mass transfer in magmatic processes IV. A revised and internally consistent thermodynamic model for the interpolation and extrapolation of liquid-solid equilibria in magmatic systems at elevated temperatures and pressures. Contrib. Mineral. Petrol. 119, 197–212. https://doi.org/10.1007/BF00307281.

Gualda, G.A.R., Ghiorso, M.S., 2015. MELTS_Excel: a Microsoft Excel-based MELTS interface for research and teaching of magma properties and evolution. Geochem. Geophys. Geosyst. 16, 315–324. https://doi.org/10.1002/2014GC005545.

Hackman, B., 1988. Geology of the Baringo-Laikipia Area: Degree Sheet 35 with Coloured 1: 250 000 Geological Map and Results of Geochemical Exploration. Ministry of Environment and Natural Resources, Mines and Geological Department.

Haileab, B., Brown, F.H., McDougall, I., Gathogo, P.N., 2004. Gombe Group basalts and initiation of Pliocene deposition in the Turkana depression, northern Kenya and southern Ethiopia. Geol. Mag. 141, 41–53.

Hart, W.K., Woldegabriel, G., Walter, R.C., Mertzman, S.A., 1989. Basaltic volcanism in Ethiopia: constraints on continental rifting and mantle interactions. J. Geophys. Res. Solid Earth 94, 7731–7748.

Hasterok, D., Chapman, D., 2011. Heat production and geotherms for the continental lithosphere. Earth Planet. Sci. Lett. 307, 59–70. https://doi.org/10.1016/j.epsl.2011.04.034.

Havlin, C., Parmentier, E.M., Hirth, G., 2013. Dike propagation driven by melt accumulation at the lithosphere–asthenosphere boundary. Earth Planet. Sci. Lett. 376, 20–28. https://doi.org/10.1016/j.epsl.2013.06.010.

Hayward, N., Ebinger, C., 1996. Variations in the along-axis segmentation of the Afar Rift system. Tectonics 15, 244–257.

Herzberg, C., Asimow, P.D., 2008. Petrology of some oceanic island basalts: PRIMELT2.XLS software for primary magma calculation. Geochem. Geophys. Geosyst. 9.

Herzberg, C., O'Hara, M., 2002. Plume-associated ultramafic magmas of Phanerozoic age. J. Petrol. 43, 1857–1883.

Hirschmann, M.M., Stolper, E.M., 1996. A possible role for garnet pyroxenite in the origin of the "garnet signature" in MORB. Contrib. Mineral. Petrol. 124, 185–208.

Hofmann, A.W., Jochum, K., Seufert, M., White, W.M., 1986. Nb and Pb in oceanic basalts: new constraints on mantle evolution. Earth Planet. Sci. Lett. 79, 33–45.

Hofmann, C., Courtillot, V., Feraud, G., Rochette, P., Yirgu, G., Ketefo, E., Pik, R., 1997. Timing of the Ethiopian flood basalt event and implications for plume birth and global change. Nature 389, 838–841. https://doi.org/10.1038/39853.

Iddon, F., Edmonds, M., 2020. Volatile-rich magmas distributed through the upper crust in the Main Ethiopian Rift. Geochem. Geophys. Geosyst. 21 p. e2019GC008904.

Katz, R.F., Spiegelman, M., Langmuir, C.H., 2003. A new parameterization of hydrous mantle melting. Geochem. Geophys. Geosyst. 4.

Kendall, J.-M., Stuart, G.W., Ebinger, C.J., Bastow, I.D., Keir, D., 2005. Magma-assisted rifting in Ethiopia. Nature 433, 146–148.

Kennan, P., Mitchell, J., Mohr, P., 1990. The Sagatu ridge dyke swarm, Ethiopian rift margin: revised age and new Sr-isotopic data. J. Afr. Earth Sci. 11, 39–42. https://doi.org/10.1016/0899-5362(90)90075-P.

Keranen, K., Klemperer, S.L., Gloaguen, R., Group, E.W., 2004. Three-dimensional seismic imaging of a protoridge axis in the Main Ethiopian rift. Geology 32, 949. https://doi.org/10.1130/G20737.1.

Keranen, K.M., Klemperer, S.L., Julia, J., Lawrence, J.F., Nyblade, A.A., 2009. Low lower crustal velocity across Ethiopia: is the Main Ethiopian Rift a narrow rift in a hot craton? Geochem. Geophys. Geosyst. 10 https://doi.org/10.1029/2008GC002293.

Kidane, T., Courtillot, V., Manighetti, I., Audin, L., Lahitte, P., Quidelleur, X., Gillot, P.Y., Gallet, Y., Carlut, J., Haile, T., 2003. New paleomagnetic and geochronologic results from Ethiopian Afar: Block rotations linked to rift overlap and propagation and determination of a~ 2 Ma reference pole for stable Africa. J. Geophys. Res. Solid Earth 108.

Kieffer, B., 2004. Flood and Shield Basalts from Ethiopia: magmas from the African Superswell. J. Petrol. 45, 793–834. https://doi.org/10.1093/petrology/egg112.

Kimura, J.I., Ariskin, A.A., 2014. Calculation of water-bearing primary basalt and estimation of source mantle conditions beneath arcs: PRIMACALC2 model for WINDOWS. Geochem. Geophys. Geosyst. 15, 1494–1514.

Kimura, J.-I., Kawabata, H., 2014. Trace element mass balance in hydrous adiabatic mantle melting: the Hydrous Adiabatic Mantle Melting Simulator version 1 (HAMMS1). Geochem. Geophys. Geosyst. 15, 2467–2493. https://doi.org/10.1002/2014GC005333.

Krans, S., Rooney, T., Kappelman, J., Yirgu, G., Ayalew, D., 2018. From initiation to termination: a petrostratigraphic tour of the Ethiopian Low-Ti Flood Basalt Province. Contrib. Mineral. Petrol. 173, 1–22.

Kurz, T., Gloaguen, R., Ebinger, C., Casey, M., Abebe, B., 2007. Deformation distribution and type in the Main Ethiopian Rift (MER): a remote sensing study. J. Afr. Earth Sci. 48, 100–114. https://doi.org/10.1016/j.jafrearsci.2006.10.008.

Lahitte, P., Gillot, P.Y., Kidane, T., Courtillot, V., Bekele, A., 2003. New age constraints on the timing of volcanism in central Afar, in the presence of propagating rifts. J. Geophys. Res. Solid Earth 108.

Langston, C.A., 1979. Structure under Mount Rainier, Washington, inferred from teleseismic body waves. J. Geophys. Res. Solid Earth 84, 4749–4762.

Lavayssière, A., Rychert, C., Harmon, N., Keir, D., Hammond, J.O., Kendall, J.M., Doubre, C., Leroy, S., 2018. Imaging lithospheric discontinuities beneath the northern East African Rift using S-to-P receiver functions. Geochemistry, Geophysics, Geosystems 19, 4048–4062.

Le Gall, B., Daoud, A., Maury, R., Gasse, F., Rolet, J., Jalludin, M., Moussa, N., 2015. Geological Map of the Republic of Djibouti. CERD, Djibouti.

Le Roux, V., Dasgupta, R., Lee, C.-T., 2011. Mineralogical heterogeneities in the Earth's mantle: constraints from Mn, Co, Ni and Zn partitioning during partial melting. Earth Planet. Sci. Lett. 307, 395–408.

Lee, C.-T.A., Luffi, P., Plank, T., Dalton, H., Leeman, W.P., 2009. Constraints on the depths and temperatures of basaltic magma generation on Earth and other terrestrial planets using new thermobarometers for mafic magmas. Earth Planet. Sci. Lett. 279, 20–33.

Lee, C.-T.A., Luffi, P., Chin, E.J., 2011. Building and destroying continental mantle. Annu. Rev. Earth Planet. Sci. 39, 59–90.

Maaløe, S., Aoki, K.-I., 1977. The major element composition of the upper mantle estimated from the composition of lherzolites. Contrib. Mineral. Petrol. 63, 161–173.

Mackenzie, G.D., Thybo, H., Maguire, P.K.H., 2005. Crustal velocity structure across the Main Ethiopian Rift: results from two-dimensional wide-angle seismic modelling. Geophys. J. Int. 162, 994–1006. https://doi.org/10.1111/j.1365-246X.2005.02710.x.

Maguire, P.K.H., Keller, G.R., Klemperer, S.L., Mackenzie, G.D., Keranen, K., Harder, S., Reilly, O., Thybo, H., Asfaw, L., Khan, M.A., 2006. Crustal structure of the northern Main Ethiopian Rift from the EAGLE controlled-source survey; a snapshot of incipient lithospheric break-up. Spec. Publ. Geol. Soc. Lond. 259, 269.

Mana, S., Furman, T., Carr, M., Mollel, G., Mortlock, R., Feigenson, M., Turrin, B., Swisher Iii, C., 2012. Geochronology and geochemistry of the Essimingor volcano: melting of metasomatized lithospheric mantle beneath the North Tanzanian Divergence zone (East African Rift). Lithos 155, 310–325.

Mazzarini, F., Keir, D., Isola, I., 2013a. Spatial relationship between earthquakes and volcanic vents in the central-northern Main Ethiopian Rift. J. Volcanol. Geotherm. Res. 262, 123–133.

Mazzarini, F., Rooney, T.O., Isola, I., 2013b. The intimate relationship between strain and magmatism: a numerical treatment of clustered monogenetic fields in the Main Ethiopian Rift. Tectonics 32, 49–64. https://doi.org/10.1029/2012TC003146.

McKenzie, D., Bickle, M., 1988. The volume and composition of melt generated by extension of the lithosphere. J. Petrol. 29, 625–679. https://doi.org/10.1093/petrology/29.3.625.

McKenzie, D.A.N., O'Nions, R.K., 1991. Partial melt distributions from inversion of rare earth element concentrations. J. Petrol. 32, 1021–1091. https://doi.org/10.1093/petrology/32.5.1021.

Mohr, P., 1967. Major volcano-tectonic lineament in the Ethiopian rift system. Nature 213, 664–665. https://doi.org/10.1038/213664a0.

Mohr, P., 1980. Geochemical aspects of the Sagatu ridge dike swarm, Ethiopian rift margin. In: Geodynamic Evolution of the Afro Arabian Rift System. Acad. Nat. Lincei, Atti Convegni Lincei, 47, pp. 384–406.

Mohr, P.A., Potter, E.C., 1976. The Sagatu Ridge dike swarm, Ethiopian rift margin. J. Volcanol. Geotherm. Res. 1, 55–71. https://doi.org/10.1016/0377-0273(76)90018-4.

Mohr, P., Zanettin, B., 1988. The Ethiopian flood basalt province. In: Continental Flood Basalts. Springer, pp. 63–110.

Mohr, P., Mitchell, J., Raynolds, R., 1980. Quaternary volcanism and faulting at O'a Caldera, Central Ethiopian Rift. Bull. Volcanol. 43, 173. https://doi.org/10.1007/BF02597619.

Natali, C., Beccaluva, L., Bianchini, G., Ellam, R.M., Savo, A., Siena, F., Stuart, F.M., 2016. High-MgO lavas associated to CFB as indicators of plume-related thermochemical effects: the case of ultra-titaniferous picrite–basalt from the Northern Ethiopian–Yemeni Plateau. Gondwana Res. 34, 29–48.

Nelson, W.R., Hanan, B., Graham, D.W., Shirey, S.B., Yirgu, G., Ayalew, D., Furman, T., 2019. Distinguishing plume and metasomatized lithospheric mantle contributions to post-flood basalt volcanism on the southeastern Ethiopian Plateau. J. Petrol. 60, 1063–1094.

Peccerillo, A., Barberio, M.R., Yirgu, G., Ayalew, D., Barbieri, M., Wu, T.U., 2003. Relationships between Mafic and Peralkaline Silicic Magmatism in Continental Rift Settings: a Petrological, Geochemical and Isotopic Study of the Gedemsa Volcano, Central Ethiopian Rift. J. Petrol. 44, 2003–2032. https://doi.org/10.1093/petrology/egg068.

Pik, R., Deniel, C., Coulon, C., Yirgu, G., Marty, B., 1999. Isotopic and trace element signatures of Ethiopian flood basalts: evidence for plume–lithosphere interactions. Geochim. Cosmochim. Acta 63, 2263–2279. https://doi.org/10.1016/S0016-7037(99)00141-6.

Pilet, S., Baker, M.B., Stolper, E.M., 2008. Metasomatized lithosphere and the origin of alkaline lavas. Science 320, 916–919.

Priestley, K., McKenzie, D., Debayle, E., Pilidou, S., 2008. The African upper mantle and its relationship to tectonics and surface geology. Geophys. J. Int. 175, 1108–1126.

Putirka, K.D., Perfit, M., Ryerson, F., Jackson, M.G., 2007. Ambient and excess mantle temperatures, olivine thermometry, and active vs. passive upwelling. Chem. Geol. 241, 177–206.

Reeve, M.T., Magee, C., Bastow, I.D., McDermott, C., Jackson, C.A.-L., Bell, R.E., Prytulak, J., 2021. Nature of the Cuvier Abyssal Plain crust, offshore NW Australia. J. Geol. Soc. 178, 1–17.

Ritsema, J., van Heijst, H.J., Woodhouse, J.H., 1999. Complex shear wave velocity structure imaged beneath Africa and Iceland. Science 286, 1925–1928.

Rochette, P., Tamrat, E., Féraud, G., Pik, R., Courtillot, V., Ketefo, E., Coulon, C., Hoffmann, C., Vandamme, D., Yirgu, G., 1998. Magnetostratigraphy and timing of the Oligocene Ethiopian traps. Earth Planet. Sci. Lett. 164, 497–510. https://doi.org/10.1016/S0012-821X(98)00241-6.

Rogers, N., James, D., Kelley, S., De Mulder, M., 1998. The generation of potassic lavas from the eastern Virunga province, Rwanda. J. Petrol. 39, 1223–1247.

Rooney, T.O., 2017. The Cenozoic magmatism of East-Africa: part I–Flood basalts and pulsed magmatism. Lithos. https://doi.org/10.1016/j.lithos.2017.05.014.

Rooney, T.O., 2020a. The Cenozoic Magmatism of East Africa: Part II–Rifting of the mobile belt. Lithos 105291.

Rooney, T.O., 2020b. The Cenozoic magmatism of east Africa: part IV–the terminal stages of rifting preserved in the northern East African rift system. Lithos 105381.

Rooney, T.O., 2020c. The Cenozoic magmatism of East Africa: part V–magma sources and processes in the East African Rift. Lithos 360, 105296.
Rooney, T.O., Furman, T., Yirgu, G., Ayalew, D., 2005. Structure of the Ethiopian lithosphere: Xenolith evidence in the Main Ethiopian Rift. Geochim. Cosmochim. Acta 69, 3889–3910. https://doi.org/10.1016/j.gca.2005.03.043.
Rooney, T., Furman, T., Bastow, I., Ayalew, D., Yirgu, G., 2007. Lithospheric modification during crustal extension in the Main Ethiopian Rift. J. Geophys. Res. 112 https://doi.org/10.1029/2006JB004916.
Rooney, T.O., Hanan, B.B., Graham, D.W., Furman, T., Blichert-Toft, J., Schilling, J.-G., 2012a. Upper mantle pollution during Afar Plume-continental rift interaction. J. Petrol. 53, 365–389. https://doi.org/10.1093/petrology/egr065.
Rooney, T.O., Hart, W.K., Hall, C.M., Ayalew, D., Ghiorso, M.S., Hidalgo, P., Yirgu, G., 2012b. Peralkaline magma evolution and the tephra record in the Ethiopian Rift. Contrib. Mineral. Petrol. 164, 407–426. https://doi.org/10.1007/s00410-012-0744-6.
Rooney, T.O., Herzberg, C., Bastow, I.D., 2012c. Elevated mantle temperature beneath East Africa. Geology 40, 27–30. https://doi.org/10.1130/G32382.1.
Rooney, T.O., Mohr, P., Dosso, L., Hall, C., 2013. Geochemical evidence of mantle reservoir evolution during progressive rifting along the western Afar margin. Geochim. Cosmochim. Acta 102, 65–88. https://doi.org/10.1016/j.gca.2012.08.019.
Rooney, T.O., Bastow, I.D., Keir, D., Mazzarini, F., Movsesian, E., Grosfils, E.B., Zimbelman, J.R., Ramsey, M.S., Ayalew, D., Yirgu, G., 2014. The protracted development of focused magmatic intrusion during continental rifting: focused magma intrusion during rifting. Tectonics 33, 875–897. https://doi.org/10.1002/2013TC003514.
Rooney, T.O., Morell, K.D., Hidalgo, P., Fraceschi, P., 2015. Magmatic consequences of the transition from orthogonal to oblique subduction in Panama. Geochem. Geophys. Geosyst. 16, 4178–4208.
Rooney, T.O., Lavigne, A., Svoboda, C., Girard, G., Yirgu, G., Ayalew, D., Kappelman, J., 2017a. The making of an underplate: pyroxenites from the Ethiopian lithosphere. Chem. Geol. 455, 264–281.
Rooney, T.O., Nelson, W.R., Ayalew, D., Hanan, B., Yirgu, G., Kappelman, J., 2017b. Melting the lithosphere: metasomes as a source for mantle-derived magmas. Earth Planet. Sci. Lett. 461, 105–118.
Rooney, T.O., Krans, S.R., Mège, D., Arnaud, N., Korme, T., Kappelman, J., Yirgu, G., 2018. Constraining the magmatic plumbing system in a zoned continental flood basalt province. Geochem. Geophys. Geosyst. 19, 3917–3944.
Rychert, C.A., Hammond, J.O., Harmon, N., Kendall, J.M., Keir, D., Ebinger, C., Bastow, I.D., Ayele, A., Belachew, M., Stuart, G., 2012. Volcanism in the Afar Rift sustained by decompression melting with minimal plume influence. Nat. Geosci. 5, 406.
Schilling, J.G., Kingsley, R.H., Hanan, B.B., McCully, B.L., 1992. Nd-Sr-Pb isotopic variations along the Gulf of Aden: evidence for Afar mantle plume-continental lithosphere interaction. J. Geophys. Res. Solid Earth 97, 10927–10966.
Spohn, T., Schubert, G., 1982. Convective thinning of the lithosphere: a mechanism for the initiation of continental rifting. J. Geophys. Res. Solid Earth 87, 4669–4681.
Stab, M., Bellahsen, N., Pik, R., Quidelleur, X., Ayalew, D., Leroy, S., 2015. Modes of rifting in magma-rich settings: Tectono-magmatic evolution of Central Afar. Tectonics. https://doi.org/10.1002/2015TC003893.
Stewart, K., Rogers, N., 1996. Mantle plume and lithosphere contributions to basalts from southern Ethiopia. Earth Planet. Sci. Lett. 139, 195–211.
Sun, S.-S., McDonough, W.-S., 1989. Chemical and isotopic systematics of oceanic basalts: implications for mantle composition and processes. Geol. Soc. Lond., Spec. Publ. 42, 313–345.
Thybo, H., Nielsen, C., 2009. Magma-compensated crustal thinning in continental rift zones. Nature 457, 873–876.
Trestrail, K.R., Rooney, T.O., Girard, G., Svoboda, C., Yirgu, G., Ayalew, D., Keppelman, J., 2017. Sub-continental lithospheric mantle deformation in the Yerer-Tullu Wellel Volcanotectonic Lineament: a study of peridotite xenoliths. Chem. Geol. 455, 249–263.
Trua, T., Deniel, C., Mazzuoli, R., 1999. Crustal control in the genesis of Plio-Quaternary bimodal magmatism of the Main Ethiopian Rift (MER): geochemical and isotopic (Sr, Nd, Pb) evidence. Chem. Geol. 155, 201–231. https://doi.org/10.1016/S0009-2541(98)00174-0.
Ukstins, I.A., Renne, P.R., Wolfenden, E., Baker, J., Ayalew, D., Menzies, M., 2002. Matching conjugate volcanic rifted margins: 40Ar/39Ar chrono-stratigraphy of pre- and syn-rift bimodal flood volcanism in Ethiopia and Yemen. Earth Planet. Sci. Lett. 198, 289–306.
Van Wijk, J., Van Hunen, J., Goes, S., 2008. Small-scale convection during continental rifting: evidence from the Rio Grande rift. Geology 36, 575–578.
White, R., McKenzie, D., 1989. Magmatism at rift zones: the generation of volcanic continental margins and flood basalts. J. Geophys. Res. Solid Earth 94, 7685–7729.
White, R., Smith, L., Roberts, A., Christie, P., Kusznir, N., 2008. Lower-crustal intrusion on the North Atlantic continental margin. Nature 452, 460–464.
Woldegabriel, G., Aronson, J.L., Walter, R.C., 1990. Geology, geochronology, and rift basin development in the central sector of the Main Ethiopia Rift. Geol. Soc. Am. Bull. 102, 439–458. https://doi.org/10.1130/0016-7606(1990)102<0439:GGARBD>2.3.CO;2.
Wolfenden, E., Ebinger, C., Yirgu, G., Deino, A., Ayalew, D., 2004. Evolution of the northern Main Ethiopian rift: birth of a triple junction. Earth Planet. Sci. Lett. 224, 213–228. https://doi.org/10.1016/j.epsl.2004.04.022.
Wolfenden, E., Ebinger, C., Yirgu, G., Renne, P.R., Kelley, S.P., 2005. Evolution of a volcanic rifted margin: southern Red Sea, Ethiopia. Geol. Soc. Am. Bull. 117, 846–864. https://doi.org/10.1130/B25516.1.
Yirgu, G., Ebinger, C.J., Maguire, P.K.H., 2006. The afar volcanic province within the East African Rift System: introduction. Geol. Soc. Lond., Spec. Publ. 259, 1–6.